

Combined impacts of climate change and human activities on blue and green water resources in the high-intensity development watershed

Xuejin Tan¹, Bingjun Liu^{2*}, Xuezhi Tan^{2,3*}, Zeqin Huang², Jianyu Fu²

¹ School of Geography and Planning, Sun Yat-sen University, Guangzhou, 510006, PR China

² Center of Water Resources and Environment, School of Civil Engineering, Sun Yat-sen University, Guangzhou, 510275, PR China

³ Southern Marine Science and Engineering Guangdong Laboratory (Zhuhai), Sun Yat-sen University, Zhuhai, 519082, PR China

* Corresponding authors: Bingjun Liu (liubj@mail.sysu.edu.cn)

Xuezhi Tan (tanxuezhi@mail.sysu.edu.cn)

1 Abstract

2 Sustainable management of blue and green water resources is vital for the stability and
3 sustainability of watershed ecosystems. Although there has been extensive attention to blue water
4 (*BW*) which is closely related to human beings, the relevance of green water (*GW*) for ecosystem
5 security is typically disregarded in water resource evaluations. Specifically, comprehensive studies
6 are scarce ~~there is a scarcity of comprehensive study~~ on the detection and attribution of variations
7 of blue and green water in the Dongjiang River Basin (DRB), an important source ~~for~~ of regional
8 water supply in the Guangdong-Hong Kong-Macao Greater Bay Area (GBA) of China. Here we
9 assess the variations of *BW* and *GW* scarcity, and quantify the impacts of climate change and land
10 use change on *BW* and *GW* in DRB using a multi-water-flux calibrated Soil and Water Assessment
11 Tool (SWAT). Results show that *BW* and green water storage (*GWS*) in DRB increased slowly with
12 a rate of 0.14 and 0.015 mm a⁻¹, respectively, while green water flow (*GWF*) decreased
13 significantly at a rate of -0.21 mm a⁻¹. The degree of *BW* and *GW* scarcity in DRB is low, and the
14 per capita water resources in more than 80% of DRB exceed 1700 m³ capita⁻¹ a⁻¹. Attribution
15 results show that 88.0%, 88.5%, and 39.4% of changes in *BW*, *GWF*, and *GWS* result from climate
16 change, respectively. Both climate change and land use change have decreased *BW*, while climate
17 change (land use change) have ~~decreased~~ (increased) *GWF* in DRB. These findings can guide ~~to~~
18 the optimize-optimization of the allocation of blue and green water resources between upper and
19 lower reach areas in DRB and further improve the understanding of blue and green water evolution
20 patterns in humid regions.

21 **Key words:** Blue and green water; Water scarcity; Climate change, Land use change; Water flow;

22 Dongjiang River Basin

23 **1 Introduction**

24 Land use and land cover change (LUCC)₂ and climate variability may alter hydrological
25 processes in watersheds (Berezovskaya et al., 2004; Chagas et al., 2022; Konapala et al., 2020;
26 Xuezhi Tan et al., 2022), which successively affect variations of regional water resources (Hoek
27 van Dijke et al., 2022; Pokhrel et al., 2021; Stocker et al., 2023; Suzuki et al., 2021), potentially
28 leading to ecosystem degradation and severe water shortage crises (Aghakhani Afshar et al., 2018;
29 Zuo et al., 2015). With the development of society and the economy, there is an increasing need
30 for more of water resources to ~~accommodation~~ accommodate human needs water utilization,
31 encompassing agricultural, domestic, and industrial water usage. Water scarcity and
32 spatiotemporal mismatch between regional water supply and demand in certain regions are
33 becoming increasingly severe, significantly affecting ~~the~~ sustainable development in these regions
34 (Cook et al., 2014). Quantifying water resources ~~under~~ in a changing environment is crucial for
35 guiding efficient and sustainable water use.

36 Previous studies on water resource assessment have explored the effects of climate change
37 and anthropogenic factors on available water resources, including streamflow (Tan and Gan, 2015;
38 Tan et al., 2023; Xin et al., 2019), baseflow (Ficklin et al., 2016; Tan et al., 2020), lake water
39 (Acero Triana and Ajami, 2022; Tao et al., 2020), and groundwater (Han et al., 2020). Falkenmark
40 and Rockström (2006) introduce a novel perspective on water resource assessment by categorizing
41 water resources into *BW* and *GW*. *BW* is the total of deep aquifers recharge and river streamflow,

42 such as water in lakes, and rivers. Water users such as industries, agriculture, and municipal users
43 can directly utilize *BW*. On the contrary, *GW* is the portion of precipitation that is not drained to
44 river for streamflow generation-and. *GW* is temporarily retained in the soil before eventually being
45 released back into the air by evapotranspiration. *GW* encompasses both green water flow (*GWF*)
46 and green water storage (*GWS*) (Veetil and Mishra, 2018; Zang and Liu, 2013). Traditional water
47 resource assessments ~~concentrating-concentrate~~ on available water resources— and Only-only
48 consider *BW*, but neglect *GW* (Dai et al., 2022), although *GW* is also essential. *GW* supplies about
49 80% of total water resources, sustaining crops growth and the sustainable development of forest
50 and grasslands ecosystems in arid regions or during dry seasons (Li et al., 2018; Schuol et al.,
51 2008). ~~The-g~~Green water scarcity can lead to ecosystem degradation and intensify competition
52 between human needs and ecosystems for water resources (Falkenmark et al., 2003; Veetil and
53 Mishra, 2018). Compared to traditional streamflow assessment methods, water resource scarcity
54 assessment methods based on the framework of *BW* and *GW* are more appropriate for maintaining
55 sustainable water resource management (Cooper et al., 2022; Liu et al., 2017). Recently, some
56 ~~researches-studies~~ have characterized water scarcity by assessing variations of *BW* and *GW*. For
57 example, Veetil and Mishra (2020) assess blue water scarcity and green water scarcity to show
58 the water security status of counties in the United States. Hoekstra et al. (2012) ~~uses-use~~ the concept
59 of *BW* footprint to study water scarcity issues. Schyns et al. (2019) ~~uses~~ the ~~conception-of~~ *GW*
60 footprint to investigate green water scarcity and ~~found~~ that the increasingly severe shortage of

61 *GW* poses a significant threat to natural ecosystems.

62 The ~~H~~impacts of climate change and anthropogenic on the hydrological cycle processes in
63 watersheds have attracted widespread attention (Chouchane et al., 2020; Cooper et al., 2022;
64 Sherwood and Fu, 2014; Tan and Gan, 2015; Xuejin Tan et al., 2022; Veettil and Mishra, 2016).
65 Changes in land use alter the underlying surface conditions. For example, afforestation or
66 deforestation may exacerbate or alleviate global or regional climate change, and thus affect
67 hydrological cycle processes (Bai et al., 2020; Lian et al., 2020; Qiu et al., 2023). Changes in land
68 use often lead to alterations in land-atmosphere interactions, and vegetation cover changes are
69 essential for regulating climate systems and land ecosystems (Foley et al., 2005; Huang et al.,
70 2020). Large-scale greening could modify geophysical interactions between the atmosphere and
71 the ground, impacting larger or local regional hydrological cycles. Land degradation (Walters and
72 Babbar-Sebens, 2016), deforestation (Lee et al., 2011), and urbanization (Mohan and Kandya,
73 2015; Zhang et al., 2018) also have far-reaching effects on the climate and hydrological cycle.

74 Climate change is also crucial to the variations in *BW* and *GW* resources. Precipitation is the
75 source of *BW* and *GW*, and factors such as temperature, solar radiation, and potential
76 evapotranspiration significantly influence the changes of *BW* and *GW* in ~~the basin~~watersheds,
77 especially in *GWF* (Pandey et al., 2019; Schewe et al., 2014). For a single watershed, *BW* depends
78 directly on precipitation and evapotranspiration (*GWF*) (Shen et al., 2017; Vano et al., 2012).
79 Furthermore, precipitation intensity can have a significant impact on the redistribution of

80 precipitation ~~and~~, *BW*, ~~and~~ *GW* ~~as well as~~ *GW*, by altering infiltration and runoff generation
81 processes (Eekhout et al., 2018; Nearing et al., 2005). Therefore, it is crucial to quantify the effects
82 of climate change and LUCC on *BW* and *GW* resources in a ~~basin-watershed~~ for effective water
83 resource planning and management.

84 Water resources management is the primary issue to be addressed for water security.
85 Hydrological models are important tools to meet various needs in water resource management.
86 Hydrological model simulation is an effective method to evaluate changes in blue and green water
87 resources. As a widely used semi-distributed parametric hydrological model, the SWAT model,
88 which typically subdivides watershed into smaller subbasins, is increasingly used in water
89 resources management at the watershed scale. Based on the SWAT model, researchers simulated
90 the spatiotemporal changes in blue and green water resources in Iran (Jeyrani et al., 2021), the
91 Yangtze River basin (Nie et al., 2023), the Poyang Lake basin (Liu et al., 2023), India (Sharma et
92 al., 2023). Some studies have also used model simulations to analyze the effects of climate change
93 and human activities on water resource changes in Meki River basin (Hordofa et al., 2023), China
94 (Liu et al., 2022), and Ningxia (Wu et al., 2021), etc. However, most of the hydrological models
95 used in the study were calibrated and validated using only observed streamflow data without
96 checking the accuracy of other simulated water variables, which can lead to uncertainties in
97 modeling soil moisture and evapotranspiration (Nie et al., 2023).

98 The Dongjiang River Basin (DRB) is a crucial water source ~~region~~ for core cities in GBA,

99 such as Shenzhen, Hong Kong, and Huizhou. Given the significant *BW* demand from agriculture,
100 ~~urban areas~~[domestic utilization](#), and industry, as well as the *GW* demand from over 18,000 km² of
101 forested land, the water resource stress in DRB is extremely high, although DRB is located in the
102 wet South China (Liu et al., 2018). The growing mismatch between increasing water demand and
103 decreasing water supply, along with seasonal and pollution-induced water scarcity issues, is
104 becoming increasingly prominent (Yang et al., 2018). ~~Currently~~[However](#), the majority of [current](#)
105 studies on water resources of DRB focus on changes and scarcity of surface water and groundwater
106 (*BW*) while overlooking the critical role and spatiotemporal variations of *GW* (Huang et al., 2022;
107 Jiang et al., 2023; Jiefeng Wu et al., 2021). With the high-intensity urbanization and climate change
108 in DRB, changes of *BW* and *GW* resources in DRB remain unknown.

109 This research aims to analyze the influence of climate change and LUCC on *BW* and *GW* in
110 DRB. The objectives of this research are (a) to build the SWAT model for DRB [hydrological](#)
111 [simulation](#), (b) to quantitatively evaluate the spatial and temporal variation of *BW* and *GW* in DRB,
112 (c) to assess the status of water scarcity in DRB using the framework of *BW* and *GW* resources,
113 [and](#) (d) to estimate the effects of climate change and LUCC on *BW* and *GW* in DRB.

114 **2 Materials and methods**

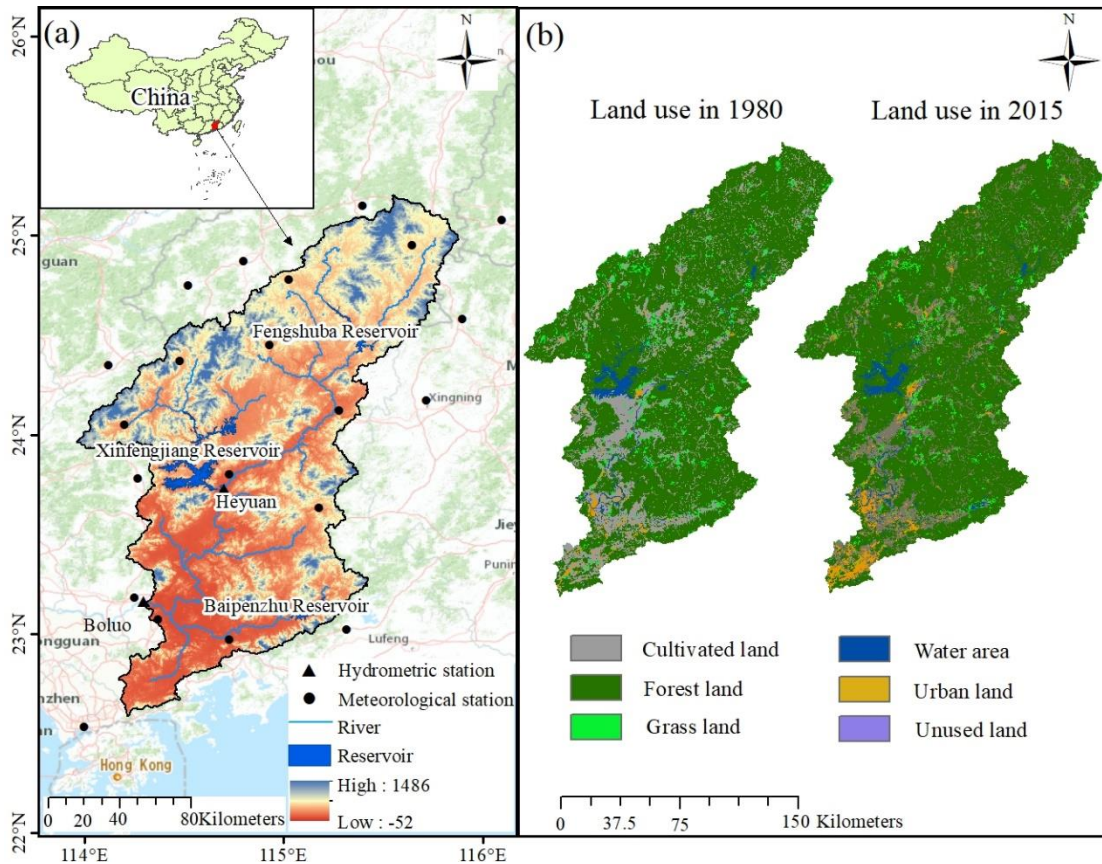
115 **2.1 Study area**

116 The Dongjiang River ~~serves as~~ an important tributary of the Pearl River, positioned between

117 longitude 113°25'-115°52'E and latitude 22°26'-25°12'N. It originates in Xunwu County, Jiangxi
118 Province, flows through Jiangxi and Guangdong provinces, and goes across major cities including
119 Longchuan, Heyuan, Dongguan, and Shenzhen. The ~~main-trunk stream~~ of the Dongjiang River
120 ~~spans-has~~ a total length of 562 km. ~~DRB covering-covers~~ a watershed area of 3.5×10^4 km². DRB
121 is ~~situated-withinof~~ the subtropical monsoon climate zone with adequate precipitation and high
122 temperatures. The average annual precipitation ranges from 1500-2400 mm, and the average
123 temperature of the basin is ~~approximately~~ 21°C (Jiefeng Wu et al., 2019). The altitude of the basin
124 decreases from ~~the~~ northeast to ~~the~~ southwest. ~~Regions of t~~The upper reaches of DRB are
125 dominated by mountains and hills, ~~those of~~ the middle reaches of DRB are dominated by hills and
126 plains, and ~~those of~~ the lower reaches of DRB are dominated by plains.

127 Previous hydrological simulation studies of DRB mainly use the Boluo hydrometric station
128 as the outlet of the watershed (He et al., 2013; Jiefeng Wu et al., 2019), so this research only
129 analyze the area of DRB where water flows to the Boluo station (Fig. 1). The Boluo hydrometric
130 station is the main control station in the lower reaches of the Dongjiang. The Boluo hydrometric
131 station ~~occupy-occupies~~ a drainage area of 25,325 km², which is 71.7% of the ~~overall-total area of~~
132 DRB. Since the 1950s, more than 896 reservoirs, ponds, dams, and other water conservancy
133 facilities have been constructed in DRB. Among them, the Baipenzhu Reservoir, Fengshuibai
134 Reservoir, and Xinfengjiang Reservoir are the ~~main-three largest~~ reservoirs in the basin with a
135 cumulative storage capacity of ~~approximately~~ 17,048 million m³. The Dongjiang-Shenzhen Water

136 Supply Project constructed in 1964 diverts water from the Dongjiang River to Shenzhen and Hong
 137 Kong for providing fresh water resources for municipal use. Over 70% of Hong Kong's freshwater
 138 supply comes from the Dongjiang River. Therefore, it is crucial to comprehend the shifts in water
 139 resources within DRB for projecting future available water resources for the development of GBA.



140
 141 Figure 1. Location and characteristics of the study area: (a) location of the watershed, spatial distribution of the
 142 hydrometeorological stations, and digital elevation model (Farr et al., 2007), (b) land use map (Xu et al.,
 143 2018).

144 2.2 Methodology

145 2.2.1 SWAT model

146 The SWAT model was adopted to simulate hydrological processes and estimate the volume

147 amount of *BW* and *GW* for DRB (Arnold et al., 1998; Neitsch et al., 2002). The SWAT model is
148 widely applied to simulate streamflow and surface runoff (Arshad et al., 2022; Martínez-Salvador
149 and Conesa-García, 2020; Nie et al., 2023). The SWAT model is also widely utilized for exploring
150 ~~the~~ changes ~~of~~ in *BW* and *GW* (Dai et al., 2022; Liang et al., 2018; Schuol et al., 2008).

151 In SWAT modeling, DRB was divided into 63 sub-basins (Fig. S1), and each sub-basin was
152 then categorized into Hydrologic Response Units (HRUs) depending on land use, soils, and slope.

153 2.2.2 Model calibration and validation

154 In order to reduce the influence of hydraulic engineering, the SWAT model was calibrated
155 and validated by utilizing monthly restored natural streamflow at the Boluo and Heyuan
156 hydrometric stations. The optimum hydrological-model parameters ~~were~~ are shown in Table 1. All
157 the selected parameters are automatically calibrated with 500 simulations via SWAT-CUP. The
158 warm-up period for model simulations is the first two years of the simulation period. Restored
159 Reconstructed natural streamflow in 1970-1979 was used to calibrate the model, and monthly time
160 series of ~~restored~~ reconstructed natural streamflow, *ET* from GLEAM, and soil moisture data from
161 ERA5 during 1980-1989 were used to validate the model. The calibration period for this research
162 was 1970-1979, and the validation period was 1980-1989. Three metrics, including the
163 determination coefficient (R^2), the percentage bias (*PBIAS*), and Nash-Sutcliffe efficiency (*NSE*)
164 were applied to evaluate the simulation performance of the SWAT model:

165
$$NSE = 1 - \frac{\sum_{i=1}^n (Q_{nat} - Q_{sim})^2}{\sum_{i=1}^n (Q_{nat} - Q_{ave})^2} \quad (1)$$

166
$$PBIAS = \frac{\overline{Q_{sim}} - Q_{ave}}{Q_{ave}} \times 100 \quad (2)$$

167
$$R^2 = \left[\frac{\sum_{i=1}^n (Q_{nat} - Q_{ave})(Q_{sim} - \overline{Q_{sim}})}{\sqrt{\sum_{i=1}^n (Q_{nat} - Q_{ave})^2 \sum_{i=1}^n (Q_{sim} - \overline{Q_{sim}})^2}} \right]^2 \quad (3)$$

168

169 where Q_{nat} , Q_{ave} , Q_{sim} , and $\overline{Q_{sim}}$ are monthly natural streamflow, mean monthly natural
 170 streamflow, simulated streamflow, and mean monthly simulated streamflow, respectively, n
 171 is the [total number of](#) time step.

172 Table 1 Range of the main parameters and their optimal values [in-obtained from](#) the [model](#) calibration [period](#)

Parameter	Calibration type	Initial range	Best calibrated value
GW_REVAP.gw	V	0.19-0.2	0.199
GWQMN.gw	V	493-1247	916.493
SLSUBBSN.hru	R	2.6-5.7	2.804
ESCO.hru	V	0.89-0.97	0.901
CN2.mgt	R	0.14-0.27	0.209
CH_K2.rte	V	0.38-1.16	0.926
ALPHA_BNK.rte	V	0.12-0.18	0.165
SOL_AWC.sol	R	0.3-0.6	0.598
SOL_K.sol	R	0.32-0.69	0.669
CH_K1.sub	V	0-0.15	0.0295

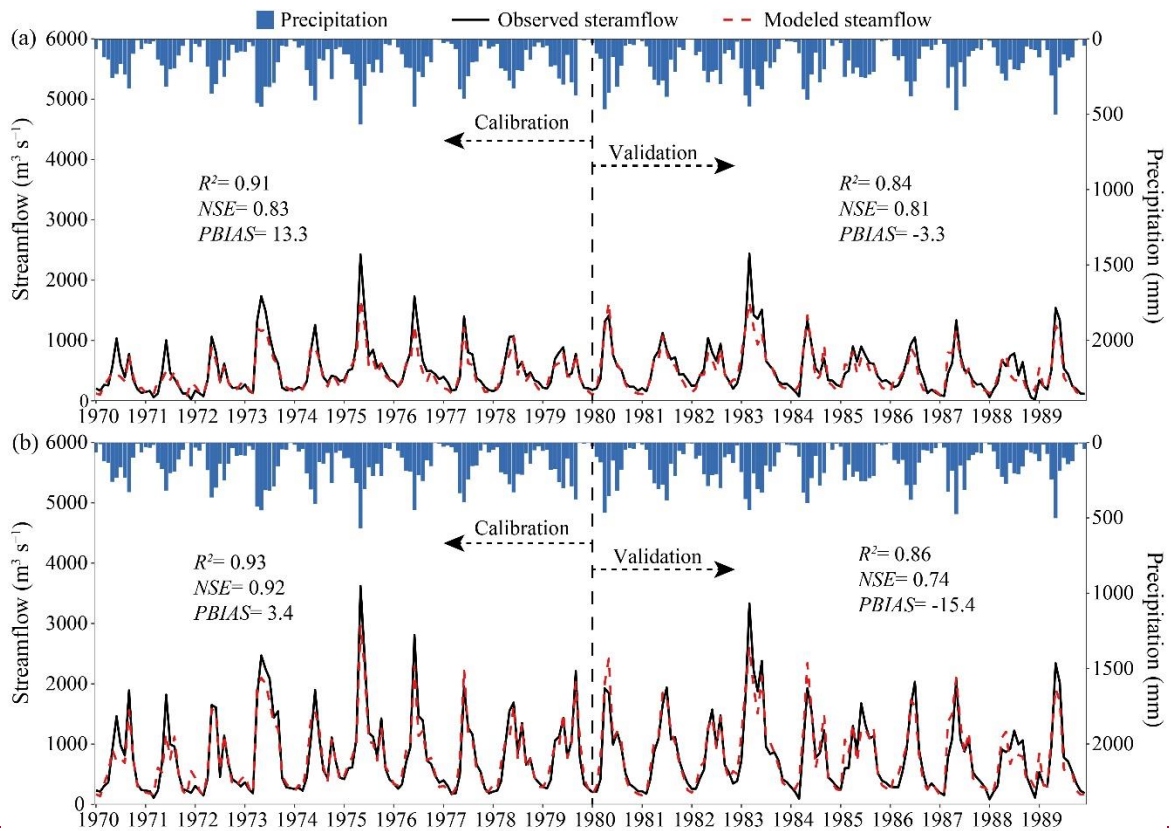
Note: The symbols of V and R denote a replacement and a relative change to the default parameter value, respectively.

173 This study reconstructed the natural monthly streamflow series of the basin by combining the
 174 inflow and outflow of the three major reservoirs (Xinfengjiang Reservoir, Fengshuba Reservoir,
 175 and Baipenzhu Reservoir) in DRB, based on the watershed water balance (Tu et al., 2018):

176
$$Q_{nat} = Q_o + \Delta Q = Q_o + Q_{in} - Q_{out} \quad (4)$$

177 where ΔQ is the total reduced water volume, Q_o , Q_{in} , and Q_{out} are the observed streamflow,
178 reservoir inflow, and reservoir outflow, respectively.

179 ~~Overall, the SWAT model shows sufficient accuracies in simulating streamflow, actual~~
180 ~~evapotranspiration, and soil moisture changes in DRB and can better simulate both seasonal and~~
181 ~~interannual changes in streamflow. During the calibration period, both stations achieved R^2 above~~
182 ~~0.9, NSE exceeding 0.8, and $PBIAS$ less than 14% (Fig. 2). Both stations had simulation streamflow~~
183 ~~R^2 greater than 0.8 during the validation period. The NSE for streamflow simulation at the Heyuan~~
184 ~~station and Boluo station of the validation were 0.81 and 0.74, respectively. The model performed~~
185 ~~well in simulating the ET and soil moisture. Since the GLEAM ET data and ERA5 soil moisture~~
186 ~~data are raster data of spatial resolution of $0.25 \times 0.25^\circ$, considering the influence of data accuracy~~
187 ~~on the results, this study uses the watershed scale to validate the simulation results of ET and soil~~
188 ~~moisture. In the validation period, the R^2 and NSE for the simulation of evapotranspiration were~~
189 ~~0.92 and 0.8, respectively (Fig. S1), while the R^2 and the NSE for the soil moisture simulation were~~
190 ~~both greater than 0.6. These validation results show that the model can be used to simulate~~
191 ~~hydrological regimes in DRB.~~



192
193 ~~Figure 2. Simulated and observed monthly streamflow at the (a) Heyuan and (b) Boluo gauge stations~~
194 ~~during calibration and validation periods.~~

195 ~~2.3 Scenario design and simulation~~

196

197 ~~Table 2 Scenario settings for the simulation of effects of climate change and LUC on blue and green water~~

Scenarios	Land use	Climate period	Combined effects	Land-use change effects	Climate change effects
S1	1980	1970-1993			
S2	1980	1994-2017			S2-S1
S3	2015	1994-2017	S3-S1	S3-S2	

198 2.4.3 Calculation of blue and green water and water security indicators

199 2.3.1 Calculation of blue and green water

200 *BW* is calculated from the sum of water yield (SWAT output WYLD) and groundwater storage.
201 The former refers to the amount of water that leaves the HRU and enters the channel. The latter
202 represents the net amount of water recharged to aquifers (SWAT output GW_RCHG) and the
203 amount of aquifer water discharges to the main channel (SWAT output GW_W) during a time step
204 (Hordofa et al., 2023). *GW* can be divided into two components including *GW_F* which is the actual
205 evapotranspiration (SWAT output ET) from the HRU, and *GW_S* which is the soil water moisture
206 (SWAT output SW) (Nie et al., 2023; Veettil and Mishra, 2018). The calculation of the Green Water
207 Index (*GWI*) involves dividing the quantity of *GW* by the sum of *BW* and *GW* (Ding et al., 2024;
208 Nie et al., 2023).

209 2.4.3.1.2 Blue and green water scarcity

210 Blue water scarcity (*BWSC*) is determined by the quotient of *BW* withdrawal and availability.
211 The estimation of *BW* withdrawals (~~*BWR*~~*BWW*) in this study involved the multiplication of the
212 aggregate population in each sub-basin by the combined water consumption per person (Liang et
213 al., 2020). The population of each sub-basin was extracted from the population raster data. ~~*BW*~~
214 Blue water availability (*BWA*) represents the quantity of water that can be utilized without
215 negatively impacting the river ecosystems. Exhaustive exploitation of *BW* in rivers may adversely
216 impacts river ecosystems. Previous studies have generally used environmental flow requirements
217 (~~*EFQEFR*~~) as a suitable metric for sustaining robust ecosystems (Honrado et al., 2013). According

218 to the study of Richter (2010) and Richter et al. (2012), extracting more than 20% of the water
 219 from rivers may result in ecological degradation. Therefore, 20% of streamflow can be deemed
 220 BW and used for water supply (Veettil and Mishra, 2016). The calculation of EFR , BWA , and $BWSC$
 221 are as follows:

$$222 \quad EFR_{(a,t)} = 0.8 \times Q_{\text{mean}(a,t)} \quad (6)$$

223 where $EFQ_{(a,t)}$ is the $EFQ - EFR$ for sub-basin 'a' during time 't'; Q_{mean} is the long-term
 224 monthly average streamflow.

$$225 \quad BWA_{(a,t)} = Q_{(a,t)} - EFQ_{(a,t)} \quad (7)$$

$$226 \quad BWSC = BWW / BWA \quad (8)$$

227 Green water scarcity ($GWSC$) is defined as the ratio between green water footprint ($GWFO$)
 228 and green water availability (GWA). ~~The~~ $GWFO$ denotes the actual evapotranspiration from the
 229 watershed. GWA is the soil moisture that is available for evapotranspiration and vegetation
 230 transpiration and is equal to the initial soil moisture (Liang et al., 2020). The $GWSC$ can be
 231 formulated as:

$$232 \quad GWSC_{(a,t)} = GWFO_{(a,t)} / GWA_{(a,t)} \quad (9)$$

233 where $GWSC$ is green water scarcity; $GWFO_{(x,t)}$ is the actual evapotranspiration; $GWA_{(a,t)}$ is initial
 234 soil moisture.

235 2.43.2-3 Regional water stress

236 The Falkenmark index (FLK) (Falkenmark et al., 1989) is a widely used measures of water

237 stress, defined as the proportion of *BWA* to the overall population. The Falkenmark index is
 238 classified into no stress, stress, scarcity, and absolutely scarcity based on per capita water use.
 239 Absolute scarcity is regarded to occur in areas where the indicator threshold is less than 500 m³
 240 capita⁻¹ a⁻¹, and no stress is thought to occur in areas where the threshold is larger than 1700 m³
 241 capita⁻¹ a⁻¹.

242 2.5.4 Calculation of relative contribution

243 2.4.1 Scenario design and simulation

244 Three scenarios were constructed to assess the impacts of climate change and LUCC on *BW*
 245 and *GW* by changing climate conditions (land use) while holding land use (climate conditions) for
 246 the three scenarios simulation each (Table 2). The land use map was fixed when simulating the
 247 influences of climate change on blue and green water (S2-S1), while climate conditions was fixed
 248 when simulating the influences of LUCC on blue and green water (S3-S2). The climate conditions
 249 and the land use were altered when assessing the joint influences of climate change and LUCC on
 250 blue and green water (S3-S1).

251 Table 2 Scenario settings for the simulation of effects of climate change and LUCC on blue and green water

<u>Scenarios</u>	<u>Land use</u>	<u>Climate period</u>	<u>Combined effects</u>	<u>Land use change effects</u>	<u>Climate change effects</u>
<u>S1</u>	<u>1980</u>	<u>1970-1993</u>			
<u>S2</u>	<u>1980</u>	<u>1994-2017</u>			<u>S2-S1</u>
<u>S3</u>	<u>2015</u>	<u>1994-2017</u>	<u>S3-S1</u>	<u>S3-S2</u>	

252 2.4.2 Relative contribution rate calculation

253 The influences of climate change and LUCC on the changes of blue and green water in
254 different periods are evaluated utilizing the relative contribution (RC) rate in this research (Li et
255 al., 2021):

256 Climate change contribution to *BW* and *GW* change is estimated by:

$$257 \quad RC_C = \frac{|X_2 - X_1|}{|X_2 - X_1| + |X_3 - X_2|} \times 100\% \quad (10)$$

258 where X_1 , X_2 , and X_3 are the amount of water including *BW* or *GW* and *GWS*, respectively
259 for scenario *S1*, *S2*, and *S3*.

260 The contribution of LUCC to changes in *BW* and *GW* are estimated by Equations 11.

$$261 \quad RC_L = \frac{|X_3 - X_2|}{|X_3 - X_2| + |X_2 - X_1|} \times 100\% \quad (11)$$

262 2.5 Data

263 The dataset used in this study consists of three parts: (1) hydrometeorological data, (2)
264 geospatial data encompassing DEM, soil type, and land use, and (3) socioeconomic data
265 encompassing per capita water consumption and population data.

266 Observed monthly streamflow data of the two hydrological stations in the study were
267 collected for the years 1970-2000 from Boluo Station and Heyuan Station, and the observed
268 streamflow time series of these two hydrological stations are of no missing data. Monthly inflow

269 and outflow data of the three major reservoirs in DRB were also collected. All hydrologic data
270 were obtained from the Guangdong Provincial Hydrological Bureau. Meteorological data of daily
271 precipitation, temperature, and other meteorological data for 1968-2017 from 21 Meteorological
272 stations in the watershed were obtained from the National Meteorological Information Center of
273 the China Meteorological Administration. Monthly actual *ET* data for SWAT model validation was
274 obtained from the Amsterdam Evapotranspiration Model dataset with a spatial resolution of 0.25°
275 $\times 0.25^\circ$ (Martens et al., 2017). Monthly soil moisture data for SWAT model validation was obtained
276 from the European Center for Medium-Range Weather Forecasts ERA5-land dataset with a spatial
277 resolution of $0.1^\circ \times 0.1^\circ$ (Muñoz Sabater, 2019). The actual evapotranspiration and soil moisture
278 of the watershed equals to the average of all grids included in DRB.

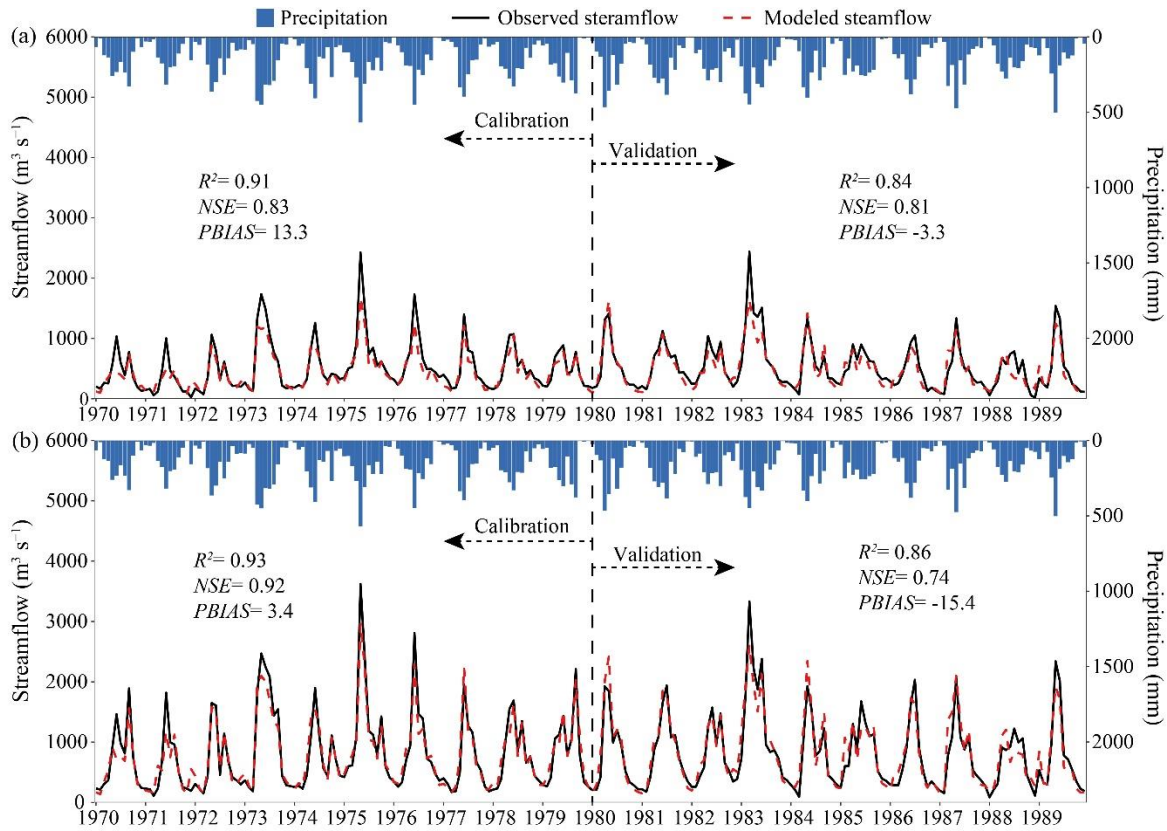
279 The ~~90-90~~-meter resolution DEM data and ~~30-30~~-meter resolution land use data at ten-year
280 intervals (i.e., 1980, 1990, 2000, 2010, 2015) are obtained from the Data Center for Resources and
281 Environmental Sciences of the Chinese Academy of Sciences (Xu et al., 2018). Soil data is
282 obtained from the 1-km resolution Harmonized World Soil Database dataset from the Food and
283 Agriculture Organization of the United Nations (Fischer et al., 2008).

284 The annual per capita integrated water consumption data of DRB from 2000-2017 was
285 acquired from the Water Resources Bulletin of Guangdong Province. The population data in 2000,
286 2005, 2010, and 2015 was obtained from the 1×1 km spatial raster data of the Resource and
287 Environment Science and Data Center of the Chinese Academy of Sciences (Xu, 2017).

288 **3 Results**

289 3.1 Model Performance

290 The SWAT model shows sufficient accuracies in simulating streamflow, actual
291 evapotranspiration, and soil moisture changes in DRB and can better simulate both seasonal and
292 interannual changes in streamflow. During the calibration period, both stations achieved R^2 above
293 0.9, NSE exceeding 0.8, and $PBIAS$ less than 14% (Fig. 2). Both stations had simulated streamflow
294 R^2 greater than 0.8 during the validation period. The NSE for streamflow simulation at the Heyuan
295 station and Boluo station of the validation were 0.81 and 0.74, respectively. The model performs
296 well in simulating the ET and soil moisture. Since the GLEAM ET data and ERA5 soil moisture
297 data are raster data of spatial resolution of $0.25 \times 0.25^\circ$, considering the influence of data accuracy
298 on the results, this study uses the watershed scale to validate the simulation results of ET and soil
299 moisture. In the validation period, the R^2 and NSE for the simulation of evapotranspiration were
300 0.92 and 0.8, respectively (Fig. S2), while the R^2 and the NSE for the soil moisture simulation were
301 both greater than 0.6. These validation results show that the model can be used to simulate
302 hydrological regimes in DRB.



303
304 Figure 2. Simulated and observed monthly streamflow at the (a) Heyuan and (b) Boluo gauge stations
305 during calibration and validation periods.

306
307 **3.1.2 LUCC and Climate variability in DRB**

308 LUCC in DRB is mainly the decrease of cultivated land and the increase of urban land. The
309 land use in DRB primarily consisted of forest land (18,875-18833 km²), which is more than 70%
310 of DRB. From 1980 to 2015, the urban land and water areas showed an increase of 469.4 km²
311 (137%) and 17.4 km² (2.8%), while the grassland, cultivated land, and forest land showed a
312 decrease of 41.3 (4.3%), 487.5 (10.8%), and 42.1 km² (0.2%), respectively (Table 3).

313 Table 3 Land use transfer matrix in DRB from 1980 to 2015

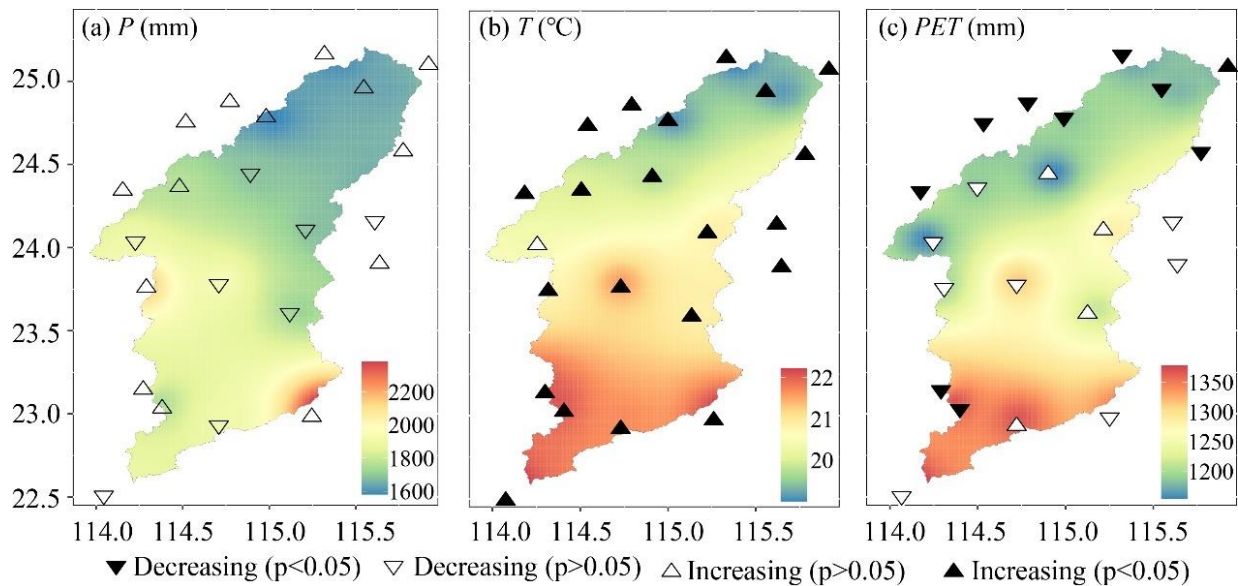
Land use type	2015						1980 total (km ²)
	Grass Land (km ²)	Urban land (km ²)	Cultivated Land (km ²)	Forest land (km ²)	Water area (km ²)	Unused land (km ²)	
1980 Grassland	795.6	29.9	18.3	123.5	2.5	0.0	969.7
Urban land	0.6	319.6	12.4	7.6	2.3	0.0	342.4
Cultivated land	19.0	269.8	3771.7	427.9	40.4	0.03	4528.8
Forest land	110.7	183.7	226.2	18278.7	33.1	0.02	18832.5
Water area	2.5	8.9	12.7	36.8	551.0	0.00	611.9
Unused land	0.0	0.0	0.02	0.03	0.00	0.45	0.51
2015 total	928.4	811.9	4041.3	18874.5	629.2	0.51	25285.8

314 DRB exhibited significant regional differences in multi-year average precipitation,
315 temperature, and potential evapotranspiration. The precipitation exhibited an increasing trend from
316 the central to the south and north of DRB. The temperature and potential evapotranspiration
317 showed an overall distribution pattern of greater values in the south and minor values in the north
318 of DRB (Fig. 3). The multi-year average precipitation for the entire of DRB was 1790.1 mm, with
319 annual precipitation ranging from 1236.2-2567.5 mm. The regions with the highest multi-year
320 average annual precipitation are located in the southeast of DRB, where annual precipitation
321 exceeds 2200 mm, while the regions with the lowest precipitation are in the northeastern of the
322 watershed. The average annual temperature in DRB ranged from 19.5-21.3 °C, and the average
323 annual potential evapotranspiration ranged from 1101.5-1320.6 mm. The south of DRB is
324 predominantly urban, characterized by the urban heat island effect, while the north of DRB is
325 mountainous with higher elevations, leading to the spatial distribution of temperatures.

326 The average temperature and potential evapotranspiration at DRB meteorological stations

327 exhibited significant variations, while precipitation showed a relatively minor trend (Fig. 3).
 328 Overall, basin-averaged precipitation and potential evapotranspiration showed a non-significant
 329 decreasing trend, while temperatures showed a significant increasing trend. There was no
 330 significant change trend of precipitation for all stations in DRB (Fig. 3a). Twenty out of 21
 331 meteorological stations in the region showed statistically significant increasing trends in average
 332 temperature, indicating a warming trend (Fig. 3b). Nine stations showed a significant decreasing
 333 trend in potential evapotranspiration, primarily located in northern DRB (Fig. 3c).

334



335
 336 Figure 3. Spatial distribution of annual mean (a) precipitation, (b) temperature, (c) potential
 337 evapotranspiration in DRB from 1960-2017. Each triangle represents the Mann-Kendall test result at a
 338 meteorological station.

339 The mean precipitation, temperature, and potential evapotranspiration of DRB can be
 340 obtained from the precipitation, temperature, and potential evapotranspiration of stations using the
 341 Tyson polygon method. The inter-annual variation of annual precipitation in DRB showed an

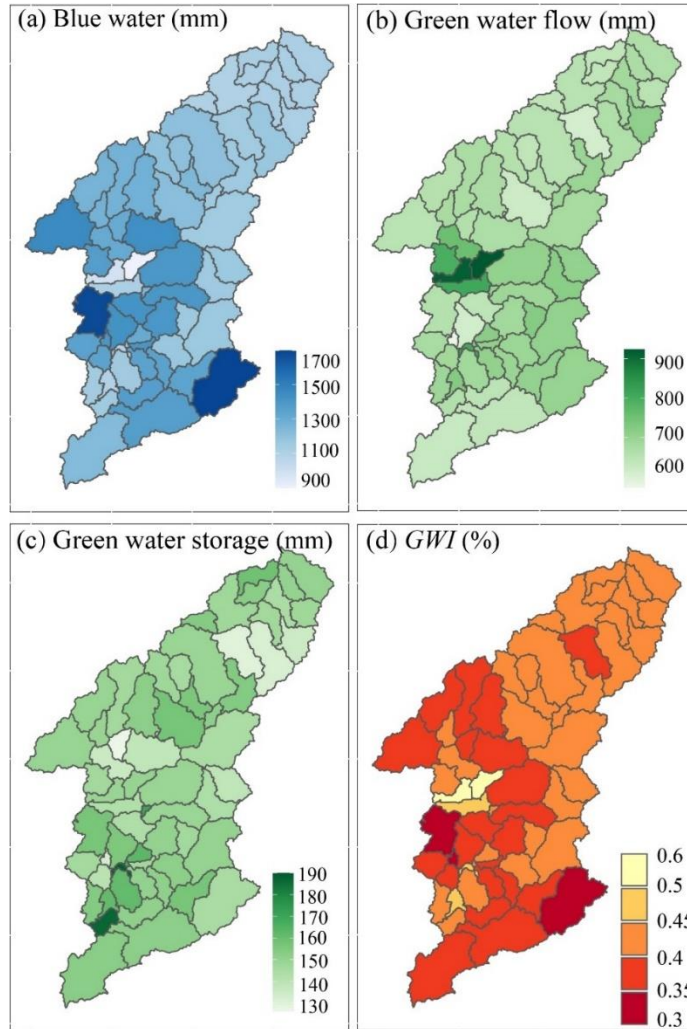
342 insignificant decreasing trend (-0.51 mm a⁻¹). The annual mean temperature showed a significant
343 increasing trend (0.024°C a⁻¹). The annual potential evapotranspiration showed a significant
344 decreasing trend (-0.38 mm a⁻¹) (Fig. S3).

345 3.2-3 Blue and green water resources

346 The average annual *BW* and *GW* were 1240.8 and 840.7 mm, respectively. The DRB water
347 resources were dominated by *BW*, representing 60.1% of the total water resources, and *BW* was
348 1.48 times higher than that of *GW* resources. The average *GWF* and *GWS* were 689.3 and 151.4
349 mm, respectively.

350 The annual *BW* resources in the sub-basins of DRB ranged from 893.7-1990 mm, showing
351 an increasing trend from the central to the south and north of DRB, aligning with the spatial
352 distribution of precipitation (Fig. 4a). The regions with abundant *BW* resources are situated in the
353 central and southeast parts of DRB (>1300 mm), and the *BW* in the upper reaches is comparatively
354 low (<1100 mm). Differences in the spatial distribution of *BW* are primarily caused by differences
355 in the spatial distribution of precipitation. Overall, the *GWF* and *GWS* are more evenly distributed
356 in the sub-basins than *BW*. The annual *GWF* in the sub-basins of DRB ranged from 573.6-923.6
357 mm. The sub-basins with higher *GWF* are primarily located in the Xinfengjiang reservoir area in
358 the middle reaches (>700 mm), while the low *GWF* sub-basins are situated in the southwest of
359 DRB (<600 mm) (Fig. 4b). The land use in the sub-basins where Xinfengjiang Reservoir is located
360 is primarily water areas, with a higher water evaporation rate than other regions, resulting in a

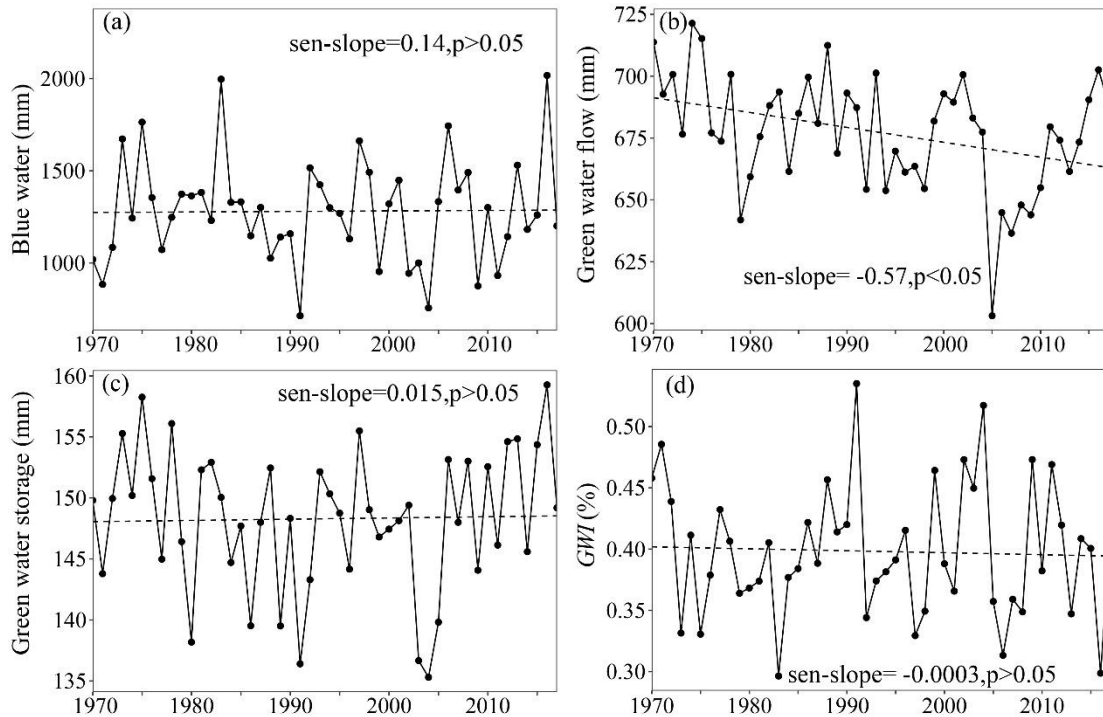
361 greater *GWF* in this area than in other regions. The annual *GWS* in the sub-basins of DRB ranged
362 from 126-190.6 mm. The sub-basins with higher *GWS* are mainly located in the lower part of DRB
363 (>150 mm) (Fig. 4c). The distribution pattern of *GWS* resources has a great relationship with the
364 soil type of the watershed. The upper reaches and the northwestern part of the watershed are mostly
365 red soil, while the middle and lower reaches are dominated by reddish soil. Reddish soil has a
366 smaller water storage capacity than red soil, loses water faster, and has weaker water conservation
367 and water supply performance than red soil. This is the primary factor for the north-south
368 discrepancies in the amount of *GWS* resources in DRB. In addition, the southern region is mostly
369 of large and medium-sized cities. As urban construction land expands, the land use type in the
370 region has gradually changed to urban land, industrial land, etc., and the solidification of road
371 surfaces has reduced the area of bare soil in the region, resulting in a decrease in *GWS* resources.
372 The annual *GWI* (Fig. 4d) showed a spatial pattern opposite to *BW*, decreasing from 0.45 in the
373 upper reaches to 0.3 in the lower reaches. The highest *GWI* is found in the upper reaches, which is
374 due to the relatively low rainfall in the upper reaches and the lush vegetation, with significant plant
375 interception and transpiration, resulting in a higher proportion of total evapotranspiration than in
376 the middle and lower reaches. The central part of the basin has the highest precipitation, leading
377 to a lower *GWI*. The southern part of the watershed has the highest temperature, and
378 evapotranspiration is high. Meanwhile, the lower reaches have a large proportion of agricultural
379 and urban land, and crop irrigation can increase evapotranspiration.



380
 381 Figure 4. Spatial distribution of mean (a) *BW*, (b) *GWF*, (c) *GWS*, (d) *GWI* in DRB over during 1970-2017.

382 In DRB, there was no significant increasing trend in either *BW* or *GWS*, while *GWF*
 383 exhibited a significant decreasing trend. The annual trend rate of *BW* in DRB was 0.14 mm a⁻¹,
 384 with an annual fluctuation range of 713.6-2017.5 mm during 1970-2017. The minimum *BW*
 385 occurred in 1991, while the maximum was recorded in 2016 (Fig. 5a). The *GWF* in DRB from
 386 1970 to 2017 exhibited a significant decreasing trend (-0.57 mm a⁻¹) (Fig. 5b). The minimum
 387 *GWF* occurred in 2005 (603.1 mm), while the maximum was recorded in 1974 (721.3 mm). In
 388 contrast, the *GWS* in DRB from 1970 to 2017 has been slowly increasing at a rate of 0.015 mm a-

389 1 (Fig. 5c). The annual fluctuation in GWS was smaller than BW and GWF. The GWI in DRB
 390 from 1970 to 2017 showed no significant decreasing trend at a rate of $-0.0003\% \text{ a}^{-1}$ ($p > 0.05$) (Fig.
 391 5d), implying that the redistribution of precipitation in DRB might change slowly.



392
 393 Figure 5. Interannual variation of (a) *BW*, (b) *GWF*, (c) *GWS*, (d) *GWI* in DRB during 1970-2017.

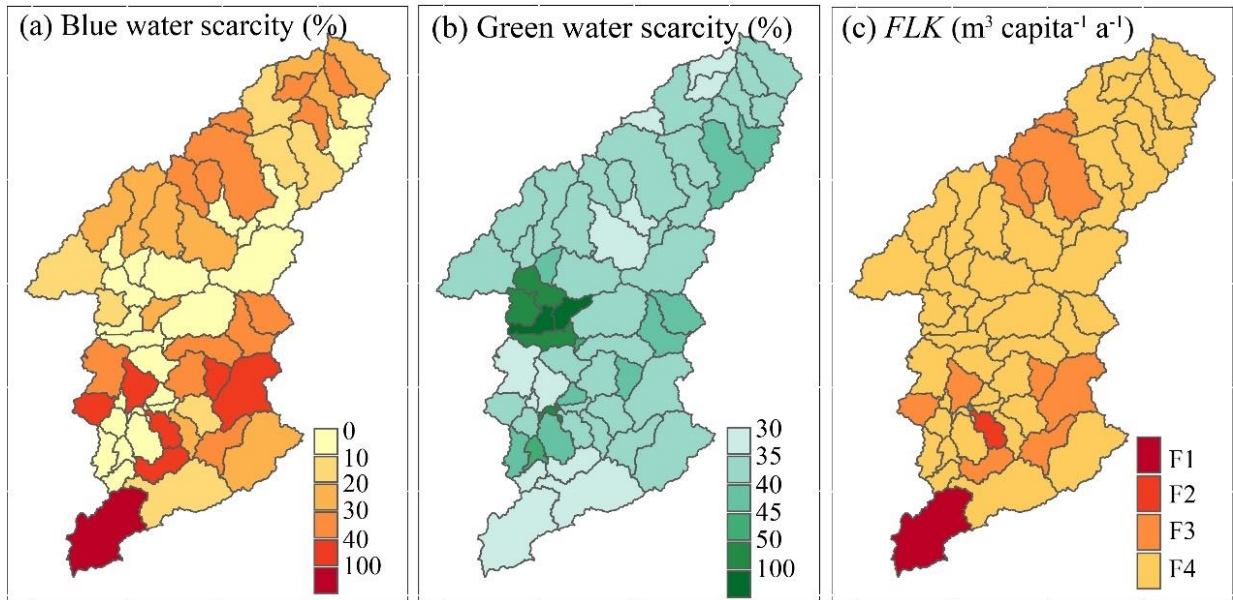
394 3.3.4 Blue and green water scarcity

395 The average blue water scarcity level in DRB was low (22.4%) during 1970-2017. The blue
 396 water scarcity levels in various sub-basins ranged from 0.1-206%. The multi-year average blue
 397 water scarcity, except for one sub-basin in the southwest, was all low (<100%) (Fig. 6a). This
 398 indicates that blue water scarcity is not common in DRB at the annual scale. Regions with
 399 relatively high blue water scarcity (>20%) are mostly situated in the upper reaches of various
 400 tributaries within the watershed, where river streamflow is relatively small. The area with the

401 highest blue water scarcity (206%) is located in the 63rd sub-basin of Shenzhen and Huizhou,
402 reaching a moderate level of blue water scarcity. This region has a large population, with a much
403 higher blue water demand than other areas. Additionally, this sub-basin is situated in the upper
404 reaches of the primary tributary of DRB, resulting in a limited supply of *BW* resources. Although
405 the northern parts of sub-basins 55, 56, and 61 have large populations, these sub-basins are situated
406 in ~~the~~ downstream of the main Dongjiang River, with a higher streamflow, leading to lower *BWSC*
407 levels. The average *GWSC* in the entire basin from 1970-2017 was low (41.4%). The blue water
408 scarcity levels in various sub-basins ranged from 31-104%. The vegetation cover in DRB is high,
409 and DRB is thus of relatively high rates of vegetation transpiration and interception evaporation.
410 The basin experiences a *GWSC* of nearly 50%, indicating a potential occurrence of *GWSC*. The
411 areas with higher *GWSC* are primarily situated in the middle reaches for DRB (Fig. 6b), where
412 water surface evaporation is high, resulting in their *GWSC* exceeding 100%. The evaporated water
413 in these areas originates from the reservoirs, not the soil, leading to an overestimation of the *GWSC*
414 in these sub-basins.

415 Furthermore, the *FLK* index was also used to quantify population-driven water resource
416 scarcity. F1-F4 represent absolute scarcity, scarcity, stress, and no stress, respectively. The results
417 showed that most regions in DRB have no water scarcity pressure (Fig. 6c). However, the 63rd
418 sub-basin experienced absolute water scarcity, and the 52nd sub-basin experienced water scarcity.
419 There were six lower reaches sub-basins and four upper reaches sub-basins facing water stress.

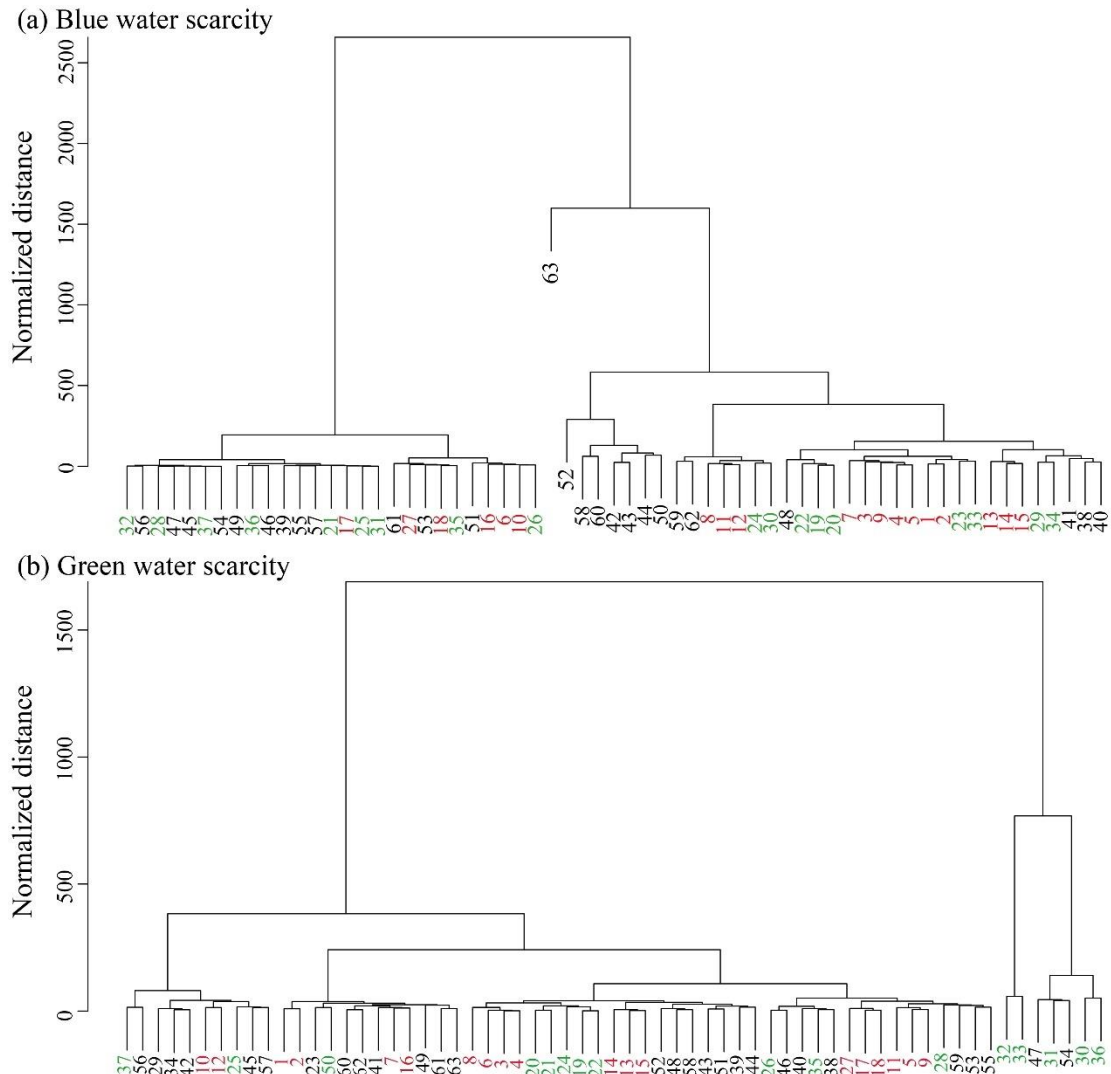
420 DRB receives ample precipitation, resulting in a relatively large river flow, generally leading to a
421 higher *FLK* index. As a result, the basin faces lower water resource pressure.



422
423 Figure 6. Spatial distribution of mean (a) *BWSC*, (b) *GWSC*, and (c) *FLK* index in DRB over during 1970-
424 2017.

425 This study also further identified hotspots of *BWSC* and *GWSC* in DRB by hierarchical
426 clustering of *BWSC* and *GWSC* in each sub-basin. Figure 7 shows the clustering tree results for
427 *BWSC* and *GWSC*. When the standardized distance was set to 500, all sub-basins could be divided
428 into four categories according to blue water scarcity: (1) The first category consisted of 27 sub-
429 basins, such as 32, 56, and 28, where the blue water scarcity level was the lowest (<20%). (2) The
430 second category comprised sub-basin 63, which has the most severe blue water scarcity (206%).
431 (3) The third category comprised seven sub-basins, such as 52, 58, and 60, all located in the lower
432 reaches, with relatively high blue water scarcity levels (40%-100%). These sub-basins are mostly
433 located in the tributaries of the lower reaches, with a relatively large population and smaller river

434 streamflow compared to the mainstem of the Dongjiang River. (4) The fourth category consisted
435 of 28 sub-basins, such as 59, 62, and 8, with blue water scarcity levels ranging from 20% to 40%.
436 Similarly, hierarchical clustering was conducted for *GWSC*. When the standardized distance was
437 set to 500, *GWSC* in the sub-basins could be divided into three categories: (1) The first category
438 consisted of 56 sub-basins, such as 37, 56, and 29, with relatively low *GWSC* levels, all below
439 50%, indicating low *GWSC*. (2) The second category consisted of sub-basins 32 and 33, where the
440 predominant land use type was water areas, leading to higher *GWSC* due to high water surface
441 evaporation. (3) The third category consisted of sub-basins 47, 31, 54, 30, and 36, where the water
442 area proportion in these sub-basins was larger than in others, leading to significant influences from
443 water surface evaporation.



444
445 Figure 7. Hierarchical clustering tree of (a) *BWSC*, (b) *GWSC*.

446 The interannual variations in *BWSC* and *GWSC* in DRB showed distinct regional differences.

447 *BWSC* in the basin was slowly increasing at a rate of $0.3\% \text{ a}^{-1}$ (Fig. 8a). The *BWSC* in the lower

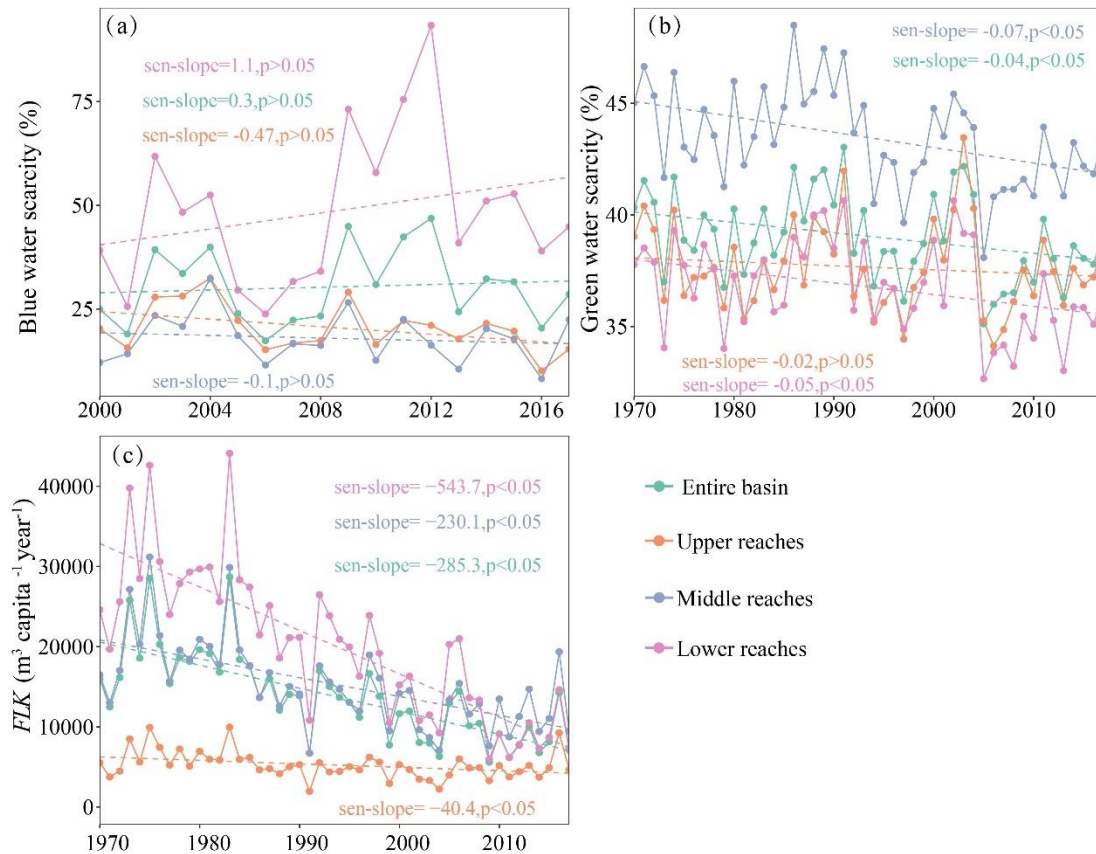
448 reaches slowly increased at a rate of $1.1\% \text{ a}^{-1}$, while the *BWSC* in the upper and middle reaches

449 slowly decreased at $-0.47\% \text{ a}^{-1}$ and $-0.1\% \text{ a}^{-1}$, respectively. *GWSC* in the upper, middle, and lower

450 reaches of DRB showed a decreasing trend, with basin scale *GWSC* decreasing significantly at a

451 rate of $-0.04\% \text{ a}^{-1}$ (Fig. 8b). Despite the acceleration of urbanization and a significant increase in

452 population in the middle and lower reaches of the watershed, blue water availability and the
 453 amount of obtainable *BW* have been increasing. Additionally, the annual per capita water
 454 consumption in the basin has decreased from 481.0 m³ in 2000 to 245.0 m³ in 2020. As a result,
 455 the rate of increase in *BWSC* in the watershed has been relatively small. In contrast, the *GWF* in
 456 DRB demonstrated a significant decreasing trend, and the *GWS* increased slowly. Therefore, the
 457 *GWSC* in DRB demonstrated a significant decreasing trend. Meanwhile, the *FLK* index of the
 458 watershed showed a significant decreasing trend (-285.3 m³ per year), which means that the per
 459 capita water resources in the watershed have significantly decreased (Fig. 8c). This is due to the
 460 rapid population growth in the watershed and the slow increase in available water resources.

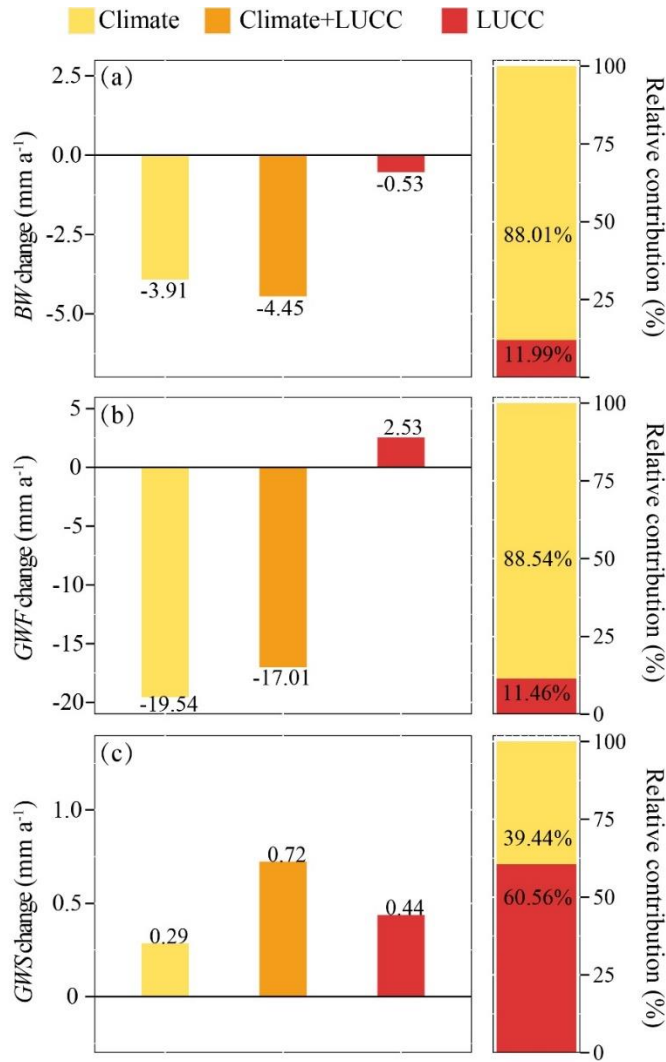


461
 462 Figure 8. Interannual variation of (a) *BWSC*, (b) *GWSC*, and (c) *FLK* index in DRB during 1970-2017.

463 3.4.5 Impacts of LUCC and climate change on blue and green water

464 To examine the impacts of climate change and LUCC on *BW* and *GW* change, this study set
465 three climate conditions and land use scenarios to explore this effect by comparing the scenarios
466 (Table 3). The combined impacts of climate change and LUCC on *BW* and *GWS* in DRB were
467 superimposed, and the combined effect on *GWF* was a negatively synergistic effect. Figure 6
468 shows the variations in *BW* and *GW* under the impacts of climate change (S2-S1) and LUCC (S3-
469 S2), as well as their combined effects (S3-S1), along with the relative contribution of climate
470 change and LUCC to the *BW* and *GW* changes in DRB during 1970-2017. Under the joint
471 influences of climate change and LUCC, *BW* decreased by 4.5 mm a⁻¹. Among this decrease,
472 climate change resulted in a loss in *BW* of 3.9 mm a⁻¹, contributing 88.0%, while LUCC led to a
473 loss in *BW* of 0.5 mm a⁻¹, contributing 12.0% (Fig. 9a). The effect of climate change on *BW*
474 variation is much greater than that of LUCC at the basin scale. Under the combined influences of
475 climate change and LUCC, *GWF* decreased by 17.0 mm a⁻¹. Among this decrease, climate change
476 accounted for a decrease in *GWF* of 19.5 mm a⁻¹, contributing 88.5% to the decrease, while LUCC
477 led to an increase in *GWF* of 2.5 mm a⁻¹, contributing 11.5% (Fig. 9b). Overall, the influence of
478 climate change on *GWF* changes in the watershed is significantly more pronounced than that of
479 LUCC. Under the joint influences of climate change and LUCC, *GWS* increased by 0.7 mm a⁻¹.
480 Among this increase, climate change contributed to an increase in *GWS* of 0.3 mm a⁻¹, accounting
481 for 39.4%, while LUCC contributed to an increase in *GWS* of 0.4 mm a⁻¹, accounting for 60.6%

482 (Fig. 9c). DRB is situated in a humid region with high *GWS*, resulting in small fluctuations of *GWS*
 483 in response to precipitation changes. The fluctuations of *GWS* are primarily influenced by the soil
 484 properties and land use. In general, the effect of climate change on the *GWS* change of DRB is
 485 smaller than the effect of LUCC.



486
 487 Figure 9. Effects and relative contribution of climate change and LUCC on the changes in (a) *BW*, (b) *GWF*,
 488 and (c) *GWS* in DRB during 1970 to 2017.

489 Under the coupled influences of climate change and LUCC, the *BW* and *GW* resources in
 490 DRB have changed. However, there were differences in the joint impacts of climate change and

491 LUCC on *BW* and *GW*. Both climate change and LUCC have led to the decrease of *BW* in the
492 watershed, and the combined effect of climate change and LUCC on *BW* equals to the sum of their
493 individual effects. Climate change, such as a decrease in potential evapotranspiration, has resulted
494 in a decrease in *GWF* in DRB, while LUCC has led to an increase in *GWF*. Therefore, the joint
495 impacts of climate change and LUCC on *GWF* was partially offset, resulting in the joint impacts
496 of climate change and LUCC on *GWF* being less than the sum of their absolute individual effects.
497 Both climate change and LUCC have led to an increase in *GWS* in DRB, and the joint impacts of
498 climate change and LUCC on *GWS* equals to the sum of their individual effects.

499 **4 Discussion**

500 This study used the SWAT model to simulate the changes in *BW* and *GW* resources in DRB
501 over the past five decades and their response to climate change and LUCC. It also assessed the
502 water resource security in the basin. ~~The results indicate that the total water resources showed a~~
503 ~~decreasing trend in the past five decades in the entire DRB mainly due to decreases in precipitation,~~
504 ~~which is similar to what Zhu et al. (2022) found.~~ The findings revealed that the *GWF* exhibited a
505 decreasing trend, and the *BW* and *GWS* exhibited an increasing trend. Liu et al. (2010) similarly
506 found an increasing trend in annual surface runoff in DRB. Potential evapotranspiration in DRB
507 showed a decreasing trend, which may be the main cause of the significant decrease in *GWF* in
508 the basin (Fig. S3), and similar conclusions are obtained in He et al. (2013).

509 We show that water resources in DRB are dominated by *BW*, with a mean annual *GWI* of 0.4,
510 which is the same as what many studies show in humid areas (Nie et al., 2023). Although the *GWI*
511 in humid areas is much smaller than that in arid areas, the ratio of *GW* in DRB still reaches 40%,
512 so it is imperative to incorporate *GW* in the water resources assessment system. The *GWI* in the
513 upper and middle reaches of DRB exceeded 0.4, while that in the lower reaches was only about
514 0.3. These results mean that to ensure the appropriate utilization of water resources, effective water
515 management in the upper and middle reaches of DRB should consider *GW* planning while water
516 management in the lower reaches should mainly consider *BW*. The assessment results of *BWSC*
517 and *GWSC* in DRB similarly illustrates this issue. The *GWSC* in the upper and middle reaches was
518 bigger than that in the lower reaches of DRB, while the *BWSC* in the lower reaches of DRB was
519 bigger than in the upper and middle reaches (Fig. 8).

520 There are robust correlations between *BW* and precipitation, *GWF* and potential
521 evapotranspiration in DRB. Climate change plays a dominant role in variations of *BW* and *GWF*.
522 *BW* is more sensitive to precipitation and potential evapotranspiration. *GWF* shows sensitivity to
523 changes in potential evapotranspiration and *GWS* is influenced by both precipitation and potential
524 evapotranspiration (He et al., 2015; Jeyrani et al., 2021). Of course, ~~there are also~~ some studies ~~for~~
525 in arid regions show that *GWF* is mainly affected by precipitation (Jun Wu et al., 2021), which
526 may be linked to the hydrothermal conditions of the basin. There is sufficient precipitation in DRB,
527 where the *GWF* changes are mainly energy-limited, and the effect of precipitation on the *GWF* is

528 smaller.

529 Although *BW* and *GW* are mainly affected by climate change, the influences of LUCC on
530 them cannot be ignored. The reaction of water resources to LUCC is exceedingly intricate and
531 involves various hydrological processes, including runoff yield, infiltration, and groundwater (Cuo,
532 2016; Zhang and Shangguan, 2016). As there is a strong compensatory effect of diverse land use
533 in the hydrological system, particularly in expansive watersheds, this could create a strong
534 resistance to *GW* and *BW* conversion (Lin et al., 2015). ~~A Decrease~~ decrease in forest land or an
535 increase in cultivated and urban land could lead to a rise in *BW* and a decline in *GW* in the
536 watershed. Veetil and Mishra (2018) demonstrate that there is a 10% rise in forest land cover and
537 a 1.4% drop in *BW*, indicating a negative elasticity between the two. However, the effect of urban
538 land on streamflow in different ~~time~~ periods showed the opposite effect. On the one hand, the
539 increase in urban land results in increases in impermeable area and thus surface runoff in the basin,
540 but at the same time, the increase in urban land may also reduce groundwater discharge to
541 streamflow. At the same time, LUCC often results in changes in vegetation. Vegetation variations
542 affect the water cycle by altering canopy interception (Shao et al., 2018; Jianping Wu et al., 2019),
543 transpiration (Chen et al., 2023) and canopy evaporation, and ameliorating soil structure (Qiu et
544 al., 2022), Thus increasing vegetation often increases infiltration and soil moisture and reduces
545 surface runoff.

546 There are several limitations and uncertainties in this research. (1) Since the quantity of the

547 *BW* and *GW* is derived from the output results of the model simulations, including water yield, *ET*,
548 soil moisture, and groundwater, the precision of the outcomes depends largely on the precision of
549 the model simulations. Given the absence of observed evapotranspiration and soil moisture data
550 for DRB, this study calibrated and validated the SWAT model using only monthly streamflow,
551 which may weaken these results to some extent. To enhance the credibility of the model, this study
552 also utilized widely used actual evapotranspiration data (GLEAM) and soil moisture (ERA5-land)
553 during model validation at a basin scale. The findings indicated that the simulation performance is
554 relatively good and meets the accuracy requirements for simulation. (2) Climate change, LUCC,
555 and large reservoir operation are the primary factors influencing the changes in hydrological
556 conditions in DRB. The contributions of reservoir regulation, LUCC, water resource utilization,
557 and climate change to the distribution of intra-annual flow are 33.5%, -9%, 4.5%, and 1%,
558 respectively, during 1956-2009 (Tu et al., 2015). The operation of reservoirs, including large
559 reservoirs like the Xinfengjiang Reservoir, is one of the important reasons for hydrological changes
560 in DRB (Lin et al., 2014; Zhang et al., 2015). The reservoir module was not established when
561 constructing the SWAT model in this research. To obtain natural *BW* and *GW* volumes in the
562 watershed and mitigate the impact of hydraulic engineering, reconstructed natural streamflow
563 based on observed flow was utilized for model calibration and validation. However, hydraulic
564 engineering significantly influences the annual allocation of *BW*. The flow restoration considered
565 the impacts of the three major reservoirs on the Dongjiang River and did not consider the impacts

566 of other minor hydraulic projects and human water consumption. (3) Both the calculations of
567 *BWSC* and the *FLK* index include environmental flows. This study represented the proportion of
568 environmental flow in streamflow as 80%. Some studies have suggested that assuming
569 environmental flow to be 80% of the total water resources in a basin may overestimate water
570 scarcity (Liu et al., 2017; Richter et al., 2012). Therefore, we varied the proportion of
571 environmental flow and assessed the degree of *BWSC* using 60% and 70% proportions. Results
572 show that only the 63rd sub-basin changed from severe *BWSC* to moderate to high *BWSC*, while
573 other sub-basins remained with low *BWSC*. Therefore, the threshold for environmental flow has a
574 minor impact on this paper. The assessment of *BWSC* and per capita water resources did not take
575 into account the water demand of cities such as Shenzhen and Hong Kong, although the water
576 supply for these cities primarily comes from the Dongjiang River through the Dongjiang-Shenzhen
577 Water Supply Project. (4) The hydrological modeling approach utilized in this research is a
578 frequently used method for quantitative analysis of attribution. Nevertheless, it implies
579 independence between climate change and LUCC and does not adequately distinguish the impacts
580 of these two components. Such restriction is diffusely recognized to exist (Dey and Mishra, 2017).
581 Despite this recognized limitation, hydrological modeling methods have been widely used in
582 numerous similar researches, yielding credible results (Li et al., 2021; Nie et al., 2023).

583 **5 Conclusion**

584 This study analyzed the spatio-temporal evolution of *BW* and *GW*, assessed the water security,
585 and evaluated the effects of climate change and LUCC on *BW* and *GW* in DRB using the SWAT
586 model. The conclusions can be outlined as follows:

587 (1) During 1970-2017, grassland, cultivated land, and forestland in DRB decreased by 4.3%,
588 10.8%, and 0.2%, respectively, while urban land and water areas increased by 137% and 2.8%,
589 respectively. The annual precipitation and potential evapotranspiration showed a non-significant
590 decreasing trend, while the annual average temperature showed a significantly increasing trend.

591 (2) The annual *BW*, *GWF*, and green storage in DRB from 1970-2017 were 1240.8 mm, 840.7
592 mm, and 151.4mm, respectively. *BW* (0.14 mm a⁻¹) and *GWS* (0.015 mm a⁻¹) in DRB showed no
593 significant increasing trend, and *GWF* (-0.57 mm a⁻¹) showed a significant decreasing trend.

594 (3) The level of annual *BWSC* and *GWSC* in DRB were low, and per capita water resources
595 exceeded 1,700 m³ capita⁻¹ a⁻¹. *BWSC* displayed a non-significant increasing trend, while the
596 *GWSC* and *FLK* index displayed a significant decreasing trend, especially in lower reaches.

597 (4) Climate change was the major driving factor of changes in *BW* and *GWF*, and LUCC was
598 the major driving factor of *GWS* change. Climate change contributed to 88.0%, 88.5%, and 39.4%
599 of the changes in *BW*, *GWF*, and *GWS* in DRB, respectively. Both climate change and LUCC
600 decrease (increase) *BW* (GWS), while climate change (LUCC) decreases (increases) *GWF* in DRB.

601 **Competing interests**

602 The contact author has declared that none of the authors has any competing interests.

603 **Acknowledgments**

604 This study was supported by the National Key Research and Development Program of China
605 (2021YFC3001000), the Science and Technology Innovation Program from Water Resources of
606 Guangdong Province (2023-01), and the National Natural Science Foundation of China (52179029,
607 52179030).

References

- Acero Triana, J.S., Ajami, H., 2022. Identifying Major Hydrologic Change Drivers in a Highly Managed Transboundary Endorheic Basin: Integrating Hydro-Ecological Models and Time Series Data Mining Techniques. *Water Resources Research* 58, e2022WR032281. <https://doi.org/10.1029/2022WR032281>
- Aghakhani Afshar, A., Hassanzadeh, Y., Pourreza-Bilondi, M., Ahmadi, A., 2018. Analyzing long-term spatial variability of blue and green water footprints in a semi-arid mountainous basin with MIROC-ESM model (case study: Kashafrud River Basin, Iran). *Theoretical and Applied Climatology* 134, 885–899. <https://doi.org/10.1007/s00704-017-2309-0>
- Arnold, J.G., Srinivasan, R., Muttiah, R.S., Williams, J.R., 1998. Large Area Hydrologic Modeling and Assessment Part I: Model Development1. *JAWRA Journal of the American Water Resources Association* 34, 73–89. <https://doi.org/10.1111/j.1752-1688.1998.tb05961.x>
- Arshad, A., Mirchi, A., Samimi, M., Ahmad, B., 2022. Combining downscaled-GRACE data with SWAT to improve the estimation of groundwater storage and depletion variations in the Irrigated Indus Basin (IIB). *Science of The Total Environment* 838, 156044. <https://doi.org/10.1016/j.scitotenv.2022.156044>
- Bai, X., Jia, X., Jia, Y., Shao, M., Hu, W., 2020. Modeling long-term soil water dynamics in response to land-use change in a semi-arid area. *Journal of Hydrology* 585, 124824. <https://doi.org/10.1016/j.jhydrol.2020.124824>
- Berezovskaya, S., Yang, D., Kane, D.L., 2004. Compatibility analysis of precipitation and runoff trends over the large Siberian watersheds. *Geophysical Research Letters* 31. <https://doi.org/10.1029/2004GL021277>
- Chagas, V.B.P., Chaffé, P.L.B., Blöschl, G., 2022. Climate and land management accelerate the Brazilian water cycle. *Nat Commun* 13, 5136. <https://doi.org/10.1038/s41467-022-32580-x>
- Chen, Z., Wang, W., Cescatti, A., Forzieri, G., 2023. Climate-driven vegetation greening further reduces water availability in drylands. *Global Change Biology* 29, 1628–1647. <https://doi.org/10.1111/gcb.16561>
- Chouchane, H., Krol, M.S., Hoekstra, A.Y., 2020. Changing global cropping patterns to minimize national blue water scarcity. *Hydrology and Earth System Sciences* 24, 3015–3031. <https://doi.org/10.5194/hess-24-3015-2020>
- Cook, B.I., Smerdon, J.E., Seager, R., Coats, S., 2014. Global warming and 21 st century drying. *Climate Dynamics* 43, 2607–2627. <https://doi.org/10.1007/s00382-014-2075-y>
- Cooper, C.M., Troutman, J.P., Awal, R., Habibi, H., Fares, A., 2022. Climate change-induced variations in blue and green water usage in U.S. urban agriculture. *Journal of Cleaner Production* 348, 131326. <https://doi.org/10.1016/j.jclepro.2022.131326>
- Cuo, L., 2016. Land use/cover change impacts on hydrology in large river basins: a review. *Terrestrial Water Cycle and Climate Change: Natural and Human-Induced Impacts* 221, 103.

- <https://doi.org/10.1002/9781118971772.ch6>
- Dai, C., Qin, X., Dong, F., Cai, Y., 2022. Climate change impact on blue and green water resources distributions in the Beijiang River basin based on CORDEX projections. *Journal of Water and Climate Change* 13, 2780–2798. <https://doi.org/10.2166/wcc.2022.115>
- Dey, P., Mishra, A., 2017. Separating the impacts of climate change and human activities on streamflow: A review of methodologies and critical assumptions. *Journal of Hydrology* 548, 278–290. <https://doi.org/10.1016/j.jhydrol.2017.03.014>
- Ding, B., Zhang, J., Zheng, P., Li, Z., Wang, Y., Jia, G., Yu, X., 2024. Water security assessment for effective water resource management based on multi-temporal blue and green water footprints. *Journal of Hydrology* 632, 130761. <https://doi.org/10.1016/j.jhydrol.2024.130761>
- Eekhout, J.P.C., Hunink, J.E., Terink, W., de Vente, J., 2018. Why increased extreme precipitation under climate change negatively affects water security. *Hydrology and Earth System Sciences* 22, 5935–5946. <https://doi.org/10.5194/hess-22-5935-2018>
- Falkenmark, M., Folke, C., Falkenmark, Malin, 2003. Freshwater as shared between society and ecosystems: from divided approaches to integrated challenges. *Philosophical Transactions of the Royal Society of London. Series B: Biological Sciences* 358, 2037–2049. <https://doi.org/10.1098/rstb.2003.1386>
- Falkenmark, M., Lundqvist, J., Widstrand, C., 1989. Macro-scale water scarcity requires micro-scale approaches. *Natural Resources Forum* 13, 258–267. <https://doi.org/10.1111/j.1477-8947.1989.tb00348.x>
- Falkenmark, M., Rockström, J., 2006. The New Blue and Green Water Paradigm: Breaking New Ground for Water Resources Planning and Management. *Journal of Water Resources Planning and Management* 132, 129–132. [https://doi.org/10.1061/\(ASCE\)0733-9496\(2006\)132:3\(129\)](https://doi.org/10.1061/(ASCE)0733-9496(2006)132:3(129))
- Farr, T.G., Rosen, P.A., Caro, E., Crippen, R., Duren, R., Hensley, S., Kobrick, M., Paller, M., Rodriguez, E., Roth, L., Seal, D., Shaffer, S., Shimada, J., Umland, J., Werner, M., Oskin, M., Burbank, D., Alsdorf, D., 2007. The Shuttle Radar Topography Mission. *Reviews of Geophysics* 45. <https://doi.org/10.1029/2005RG000183>
- Ficklin, D.L., Robeson, S.M., Knouft, J.H., 2016. Impacts of recent climate change on trends in baseflow and stormflow in United States watersheds. *Geophys Res Lett* 43, 5079–5088. <https://doi.org/10.1002/2016gl069121>
- Fischer, G., Nachtergaele, F., Prieler, S., Van Velthuizen, H.T., Verelst, L., Wiberg, D., 2008. Global agro-ecological zones assessment for agriculture (GAEZ 2008). IIASA, Laxenburg, Austria and FAO, Rome, Italy 10.
- Foley, J.A., DeFries, R., Asner, G.P., Barford, C., Bonan, G., Carpenter, S.R., Chapin, F.S., Coe, M.T., Daily, G.C., Gibbs, H.K., 2005. Global consequences of land use. *Science* 309, 570–574. <https://doi.org/10.1126/science.1111772>
- Han, Z., Huang, S., Huang, Q., Bai, Q., Leng, G., Wang, H., Zhao, J., Wei, X., Zheng, X., 2020. Effects of vegetation restoration on groundwater drought in the Loess Plateau, China. *Journal of Hydrology* 591, 125566. <https://doi.org/10.1016/j.jhydrol.2020.125566>
- He, Y., Lin, K., Chen, X., 2013. Effect of Land Use and Climate Change on Runoff in the Dongjiang Basin of South China. *Mathematical Problems in Engineering* 2013, e471429.

- <https://doi.org/10.1155/2013/471429>
- He, Y., Lin, K., Chen, X., Ye, C., Cheng, L., 2015. Classification-Based Spatiotemporal Variations of Pan Evaporation Across the Guangdong Province, South China. *Water Resour Manage* 29, 901–912. <https://doi.org/10.1007/s11269-014-0850-5>
- Hoek van Dijke, A.J., Herold, M., Mallick, K., Benedict, I., Machwitz, M., Schlerf, M., Pranindita, A., Theeuwens, J.J.E., Bastin, J.-F., Teuling, A.J., 2022. Shifts in regional water availability due to global tree restoration. *Nature Geoscience* 15, 363–368. <https://doi.org/10.1038/s41561-022-00935-0>
- Hoekstra, A.Y., Mekonnen, M.M., Chapagain, A.K., Mathews, R.E., Richter, B.D., 2012. Global Monthly Water Scarcity: Blue Water Footprints versus Blue Water Availability. *PLOS ONE* 7, e32688. <https://doi.org/10.1371/journal.pone.0032688>
- Honrado, J.P., Vieira, C., Soares, C., Monteiro, M.B., Marcos, B., Pereira, H.M., Partidário, M.R., 2013. Can we infer about ecosystem services from EIA and SEA practice? A framework for analysis and examples from Portugal. *Environmental Impact Assessment Review, Ecosystem services in EIA and SEA* 40, 14–24. <https://doi.org/10.1016/j.eiar.2012.12.002>
- Hordofa, A.T., Leta, O.T., Alamirew, T., Chukalla, A.D., 2023. Climate Change Impacts on Blue and Green Water of Meki River Sub-Basin. *Water Resour Manage* 37, 2835–2851. <https://doi.org/10.1007/s11269-023-03490-4>
- Huang, H., Xue, Y., Chilukoti, N., Liu, Y., Chen, G., Diallo, I., 2020. Assessing Global and Regional Effects of Reconstructed Land-Use and Land-Cover Change on Climate since 1950 Using a Coupled Land–Atmosphere–Ocean Model. *Journal of Climate* 33, 8997–9013. <https://doi.org/10.1175/JCLI-D-20-0108.1>
- Huang, Y., Cai, Y., Xie, Y., Zhang, F., He, Y., Zhang, P., Li, Bowen, Li, Bo, Jia, Q., Wang, Y., Qi, Z., 2022. An optimization model for water resources allocation in Dongjiang River Basin of Guangdong-Hong Kong-Macao Greater Bay Area under multiple complexities. *Science of The Total Environment* 820, 153198. <https://doi.org/10.1016/j.scitotenv.2022.153198>
- Jeyrani, F., Morid, S., Srinivasan, R., 2021. Assessing basin blue–green available water components under different management and climate scenarios using SWAT. *Agricultural Water Management* 256, 107074. <https://doi.org/10.1016/j.agwat.2021.107074>
- Jiang, J., Wang, Z., Lai, C., Wu, X., Chen, X., 2023. Climate and landuse change enhance spatio-temporal variability of Dongjiang river flow and ammonia nitrogen. *Science of The Total Environment* 867, 161483. <https://doi.org/10.1016/j.scitotenv.2023.161483>
- Konapala, G., Mishra, A.K., Wada, Y., Mann, M.E., 2020. Climate change will affect global water availability through compounding changes in seasonal precipitation and evaporation. *Nat Commun* 11, 3044. <https://doi.org/10.1038/s41467-020-16757-w>
- Lee, X., Goulden, M.L., Hollinger, D.Y., Barr, A., Black, T.A., Bohrer, G., Bracho, R., Drake, B., Goldstein, A., Gu, L., 2011. Observed increase in local cooling effect of deforestation at higher latitudes. *Nature* 479, 384–387. <https://doi.org/10.1038/nature10588>
- Li, C., Tang, G., Hong, Y., 2018. Cross-evaluation of ground-based, multi-satellite and reanalysis precipitation products: Applicability of the Triple Collocation method across Mainland China. *Journal of Hydrology* 562, 71–83. <https://doi.org/10.1016/j.jhydrol.2018.04.039>

- Li, X., Zhang, Y., Ma, N., Li, C., Luan, J., 2021. Contrasting effects of climate and LULC change on blue water resources at varying temporal and spatial scales. *Science of The Total Environment* 786, 147488. <https://doi.org/10.1016/j.scitotenv.2021.147488>
- Lian, X., Piao, S., Li, L.Z.X., Li, Y., Huntingford, C., Ciais, P., Cescatti, A., Janssens, I.A., Peñuelas, J., Buermann, W., Chen, A., Li, X., Myneni, R.B., Wang, X., Wang, Y., Yang, Y., Zeng, Z., Zhang, Y., McVicar, T.R., 2020. Summer soil drying exacerbated by earlier spring greening of northern vegetation. *Science Advances* 6, eaax0255. <https://doi.org/10.1126/sciadv.aax0255>
- Liang, J., He, X., Zeng, G., Zhong, M., Gao, X., Li, Xin, Li, Xiaodong, Wu, H., Feng, C., Xing, W., 2018. Integrating priority areas and ecological corridors into national network for conservation planning in China. *Science of the Total Environment* 626, 22–29.
- Liang, J., Liu, Q., Zhang, H., Li, Xiaodong, Qian, Z., Lei, M., Li, Xin, Peng, Y., Li, S., Zeng, G., 2020. Interactive effects of climate variability and human activities on blue and green water scarcity in rapidly developing watershed. *Journal of Cleaner Production* 265, 121834. <https://doi.org/10.1016/j.jclepro.2020.121834>
- Lin, B., Chen, X., Yao, H., Chen, Y., Liu, M., Gao, L., James, A., 2015. Analyses of landuse change impacts on catchment runoff using different time indicators based on SWAT model. *Ecological Indicators* 58, 55–63. <https://doi.org/10.1016/j.ecolind.2015.05.031>
- Lin, K., Lian, Y., Chen, X., Lu, F., 2014. Changes in runoff and eco-flow in the Dongjiang River of the Pearl River Basin, China. *Front. Earth Sci.* 8, 547–557. <https://doi.org/10.1007/s11707-014-0434-y>
- Liu, B., Peng, S., Liao, Y., Long, W., 2018. The causes and impacts of water resources crises in the Pearl River Delta. *Journal of Cleaner Production* 177, 413–425. <https://doi.org/10.1016/j.jclepro.2017.12.203>
- Liu, D., Chen, X., Lian, Y., Lou, Z., 2010. Impacts of climate change and human activities on surface runoff in the Dongjiang River basin of China. *Hydrological Processes* 24, 1487–1495. <https://doi.org/10.1002/hyp.7609>
- Liu, J., Yang, H., Gosling, S.N., Kummu, M., Flörke, M., Pfister, S., Hanasaki, N., Wada, Y., Zhang, X., Zheng, C., Alcamo, J., Oki, T., 2017. Water scarcity assessments in the past, present, and future. *Earth's Future* 5, 545–559. <https://doi.org/10.1002/2016EF000518>
- Liu, M., Wang, D., Chen, X., Chen, Y., Gao, L., Deng, H., 2022. Impacts of climate variability and land use on the blue and green water resources in a subtropical basin of China. *Sci Rep* 12, 20993. <https://doi.org/10.1038/s41598-022-21880-3>
- Liu, M., Zhang, P., Cai, Y., Chu, J., Li, Y., Wang, X., Li, C., Liu, Q., 2023. Spatial-temporal heterogeneity analysis of blue and green water resources for Poyang Lake basin, China. *Journal of Hydrology* 617, 128983. <https://doi.org/10.1016/j.jhydrol.2022.128983>
- Martens, B., Miralles, D.G., Lievens, H., Fernández-Prieto, D., Beck, H.E., Dorigo, W.A., Verhoest, N.E.C., 2017. GLEAM v3: satellite-based land evaporation and root-zone soil moisture. *Geoscientific Model Development* 10, 1903–1925. <https://doi.org/10.5194/gmd-10-1903-2017>
- Martínez-Salvador, A., Conesa-García, C., 2020. Suitability of the SWAT Model for Simulating

- Water Discharge and Sediment Load in a Karst Watershed of the Semiarid Mediterranean Basin. *Water Resour Manage* 34, 785–802. <https://doi.org/10.1007/s11269-019-02477-4>
- Mohan, M., Kandya, A., 2015. Impact of urbanization and land-use/land-cover change on diurnal temperature range: A case study of tropical urban airshed of India using remote sensing data. *Science of the Total Environment* 506, 453–465. <https://doi.org/10.1016/j.scitotenv.2014.11.006>
- Muñoz Sabater, J., 2019. ERA5-Land monthly averaged data from 1981 to present, Copernicus Climate Change Service (C3S) Climate Data Store (CDS).
- Nearing, M.A., Jetten, V., Baffaut, C., Cerdan, O., Couturier, A., Hernandez, M., Le Bissonnais, Y., Nichols, M.H., Nunes, J.P., Renschler, C.S., 2005. Modeling response of soil erosion and runoff to changes in precipitation and cover. *CATENA* 61, 131–154. <https://doi.org/10.1016/j.catena.2005.03.007>
- Neitsch, S., Arnold, J., Kiniry, J., Williams, J., King, K., 2002. Soil and water assessment tool (SWAT): theoretical documentation, version 2000. Texas Water Resources Institute, College Station, Texas, TWRI Report TR-191.
- Nie, N., Li, T., Miao, Y., Zhang, W., Gao, H., He, H., Zhao, D., Liu, M., 2023. Asymmetry of blue and green water changes in the Yangtze river basin, China, examined by multi-water-variable calibrated SWAT model. *Journal of Hydrology* 625, 130099. <https://doi.org/10.1016/j.jhydrol.2023.130099>
- Pandey, B.K., Khare, D., Kawasaki, A., Mishra, P.K., 2019. Climate Change Impact Assessment on Blue and Green Water by Coupling of Representative CMIP5 Climate Models with Physical Based Hydrological Model. *Water Resour Manage* 33, 141–158. <https://doi.org/10.1007/s11269-018-2093-3>
- Pokhrel, Y., Felfelani, F., Satoh, Y., Boulange, J., Burek, P., Gädeke, A., Gerten, D., Gosling, S.N., Grillakis, M., Gudmundsson, L., Hanasaki, N., Kim, H., Koutroulis, A., Liu, J., Papadimitriou, L., Schewe, J., Müller Schmied, H., Stacke, T., Telteu, C.-E., Thiery, W., Veldkamp, T., Zhao, F., Wada, Y., 2021. Global terrestrial water storage and drought severity under climate change. *Nat. Clim. Chang.* 11, 226–233. <https://doi.org/10.1038/s41558-020-00972-w>
- Qiu, D., Xu, R., Wu, C., Mu, X., Zhao, G., Gao, P., 2023. Effects of vegetation restoration on soil infiltrability and preferential flow in hilly gully areas of the Loess Plateau, China. *CATENA* 221, 106770. <https://doi.org/10.1016/j.catena.2022.106770>
- Qiu, D., Xu, R., Wu, C., Mu, X., Zhao, G., Gao, P., 2022. Vegetation restoration improves soil hydrological properties by regulating soil physicochemical properties in the Loess Plateau, China. *Journal of Hydrology* 609, 127730. <https://doi.org/10.1016/j.jhydrol.2022.127730>
- Richter, B.D., 2010. Re-thinking environmental flows: from allocations and reserves to sustainability boundaries. *River Research and Applications* 26, 1052–1063. <https://doi.org/10.1002/rra.1320>
- Richter, B.D., Davis, M.M., Apse, C., Konrad, C., 2012. A Presumptive Standard for Environmental Flow Protection. *River Research and Applications* 28, 1312–1321. <https://doi.org/10.1002/rra.1511>
- Schewe, J., Heinke, J., Gerten, D., Haddeland, I., Arnell, N.W., Clark, D.B., Dankers, R., Eisner,

- S., Fekete, B.M., Colón-González, F.J., Gosling, S.N., Kim, H., Liu, X., Masaki, Y., Portmann, F.T., Satoh, Y., Stacke, T., Tang, Q., Wada, Y., Wisser, D., Albrecht, T., Frieler, K., Piontek, F., Warszawski, L., Kabat, P., 2014. Multimodel assessment of water scarcity under climate change. *Proceedings of the National Academy of Sciences* 111, 3245–3250. <https://doi.org/10.1073/pnas.1222460110>
- Schuol, J., Abbaspour, K.C., Yang, H., Srinivasan, R., Zehnder, A.J., 2008. Modeling blue and green water availability in Africa. *Water resources research* 44.
- Schyns, J.F., Hoekstra, A.Y., Booij, M.J., Hogeboom, R.J., Mekonnen, M.M., 2019. Limits to the world's green water resources for food, feed, fiber, timber, and bioenergy. *Proceedings of the National Academy of Sciences* 116, 4893–4898. <https://doi.org/10.1073/pnas.1817380116>
- Shao, M., Wang, Y., Xia, Y., Jia, X., 2018. Soil drought and water carrying capacity for vegetation in the critical zone of the Loess Plateau: A review. *Vadose Zone Journal* 17, 1539–1663. <https://doi.org/10.2136/vzj2017.04.0077>
- Sharma, A., Patel, P.L., Sharma, P.J., 2023. Blue and green water accounting for climate change adaptation in a water scarce river basin. *Journal of Cleaner Production* 426, 139206. <https://doi.org/10.1016/j.jclepro.2023.139206>
- Shen, Q., Cong, Z., Lei, H., 2017. Evaluating the impact of climate and underlying surface change on runoff within the Budyko framework: A study across 224 catchments in China. *Journal of Hydrology* 554, 251–262. <https://doi.org/10.1016/j.jhydrol.2017.09.023>
- Sherwood, S., Fu, Q., 2014. A drier future? *Science* 343, 737–739. <https://doi.org/10.1126/science.1247620>
- Stocker, B.D., Tumber-Dávila, S.J., Konings, A.G., Anderson, M.C., Hain, C., Jackson, R.B., 2023. Global patterns of water storage in the rooting zones of vegetation. *Nat. Geosci.* 1–7. <https://doi.org/10.1038/s41561-023-01125-2>
- Suzuki, K., Park, H., Makarieva, O., Kanamori, H., Hori, M., Matsuo, K., Matsumura, S., Nesterova, N., Hiyama, T., 2021. Effect of Permafrost Thawing on Discharge of the Kolyma River, Northeastern Siberia. *Remote Sensing* 13, 4389. <https://doi.org/10.3390/rs13214389>
- Tan, X., Gan, T.Y., 2015. Contribution of human and climate change impacts to changes in streamflow of Canada. *Sci Rep* 5, 17767. <https://doi.org/10.1038/srep17767>
- Tan, Xuezhì, Wu, X., Huang, Z., Deng, S., Hu, M., Yew Gan, T., 2022. Detection and attribution of the decreasing precipitation and extreme drought 2020 in southeastern China. *Journal of Hydrology* 610, 127996. <https://doi.org/10.1016/j.jhydrol.2022.127996>
- Tan, Xuejin, Liu, B., Tan, Xuezhì, 2020. Global Changes in Baseflow Under the Impacts of Changing Climate and Vegetation. *Water Resources Research* 56, e2020WR027349. <https://doi.org/10.1029/2020WR027349>
- Tan, Xuejin, Liu, B., Tan, Xuezhì, Chen, X., 2022. Long-Term Water Imbalances of Watersheds Resulting From Biases in Hydroclimatic Data Sets for Water Budget Analyses. *Water Resources Research* 58, e2021WR031209. <https://doi.org/10.1029/2021WR031209>
- Tan, Xuejin, Tan, Xuezhì, Liu, B., Huang, Z., 2023. Contribution of changes in vegetation composition and climate variability on streamflow across the global watersheds. *CATENA* 232, 107394. <https://doi.org/10.1016/j.catena.2023.107394>

- Tao, S., Fang, J., Ma, S., Cai, Q., Xiong, X., Tian, D., Zhao, X., Fang, L., Zhang, H., Zhu, J., Zhao, S., 2020. Changes in China's lakes: climate and human impacts. *National Science Review* 7, 132–140. <https://doi.org/10.1093/nsr/nwz103>
- Tu, X., Singh, V.P., Chen, X., Chen, L., Zhang, Q., Zhao, Y., 2015. Intra-annual Distribution of Streamflow and Individual Impacts of Climate Change and Human Activities in the Dongjiang River Basin, China. *Water Resour Manage* 29, 2677–2695. <https://doi.org/10.1007/s11269-015-0963-5>
- Tu, X., Wu, H., Singh, V.P., Chen, X., Lin, K., Xie, Y., 2018. Multivariate design of socioeconomic drought and impact of water reservoirs. *Journal of Hydrology* 566, 192–204. <https://doi.org/10.1016/j.jhydrol.2018.09.012>
- Vano, J.A., Das, T., Lettenmaier, D.P., 2012. Hydrologic sensitivities of Colorado River runoff to changes in precipitation and temperature. *Journal of Hydrometeorology* 13, 932–949. <https://doi.org/10.1175/JHM-D-11-069.1>
- Veettil, A.V., Mishra, A., 2020. Water Security Assessment for the Contiguous United States Using Water Footprint Concepts. *Geophysical Research Letters* 47, e2020GL087061. <https://doi.org/10.1029/2020GL087061>
- Veettil, A.V., Mishra, A.K., 2018. Potential influence of climate and anthropogenic variables on water security using blue and green water scarcity, Falkenmark index, and freshwater provision indicator. *Journal of Environmental Management* 228, 346–362. <https://doi.org/10.1016/j.jenvman.2018.09.012>
- Veettil, A.V., Mishra, A.K., 2016. Water security assessment using blue and green water footprint concepts. *Journal of Hydrology* 542, 589–602. <https://doi.org/10.1016/j.jhydrol.2016.09.032>
- Walters, K.M., Babbar-Sebens, M., 2016. Using climate change scenarios to evaluate future effectiveness of potential wetlands in mitigating high flows in a Midwestern US watershed. *Ecological engineering* 89, 80–102. <https://doi.org/10.1016/j.ecoleng.2016.01.014>
- Wu, Jiefeng, Chen, X., Yu, Z., Yao, H., Li, W., Zhang, D., 2019. Assessing the impact of human regulations on hydrological drought development and recovery based on a 'simulated-observed' comparison of the SWAT model. *Journal of Hydrology* 577, 123990. <https://doi.org/10.1016/j.jhydrol.2019.123990>
- Wu, Jiefeng, Chen, X., Yuan, X., Yao, H., Zhao, Y., AghaKouchak, A., 2021. The interactions between hydrological drought evolution and precipitation-streamflow relationship. *Journal of Hydrology* 597, 126210. <https://doi.org/10.1016/j.jhydrol.2021.126210>
- Wu, Jun, Deng, G., Zhou, D., Zhu, X., Ma, J., Cen, G., Jin, Y., Zhang, J., 2021. Effects of climate change and land-use changes on spatiotemporal distributions of blue water and green water in Ningxia, Northwest China. *J. Arid Land* 13, 674–687. <https://doi.org/10.1007/s40333-021-0074-5>
- Wu, Jianping, Liu, L., Sun, C., Su, Y., Wang, C., Yang, J., Liao, J., He, X., Li, Q., Zhang, C., Zhang, H., 2019. Estimating Rainfall Interception of Vegetation Canopy from MODIS Imageries in Southern China. *Remote Sensing* 11, 2468. <https://doi.org/10.3390/rs11212468>
- Xin, Z., Li, Y., Zhang, L., Ding, W., Ye, L., Wu, J., Zhang, C., 2019. Quantifying the relative contribution of climate and human impacts on seasonal streamflow. *Journal of Hydrology*

- 574, 936–945. <https://doi.org/10.1016/j.jhydrol.2019.04.095>
- Xu, X., 2017. China population spatial distribution kilometer grid dataset. Data Registration and Publishing System of Resource and Environmental Science Data Center of Chinese Academy of Sciences.
- Xu, X., Liu, J., Zhang, S., Li, R., Yan, C., Wu, S., 2018. Multi-period land use land cover remote sensing monitoring dataset in China (CNLUCC). Resource and Environmental Science Data Registration and Publication System. (<http://www.resdc.cn/DOI>). <https://doi.org/DOI:10.12078/2018070201>
- Yang, L.E., Chan, F.K.S., Scheffran, J., 2018. Climate change, water management and stakeholder analysis in the Dongjiang River basin in South China. *International Journal of Water Resources Development* 34, 166–191. <https://doi.org/10.1080/07900627.2016.1264294>
- Zang, C., Liu, J., 2013. Trend analysis for the flows of green and blue water in the Heihe River basin, northwestern China. *Journal of Hydrology* 502, 27–36. <https://doi.org/10.1016/j.jhydrol.2013.08.022>
- Zhang, Q., Gu, X., Singh, V.P., Chen, X., 2015. Evaluation of ecological instream flow using multiple ecological indicators with consideration of hydrological alterations. *Journal of Hydrology* 529, 711–722. <https://doi.org/10.1016/j.jhydrol.2015.08.066>
- Zhang, Y., Shangguan, Z., 2016. The change of soil water storage in three land use types after 10years on the Loess Plateau. *CATENA* 147, 87–95. <https://doi.org/10.1016/j.catena.2016.06.036>
- Zhang, Yongyong, Xia, J., Yu, J., Randall, M., Zhang, Yichi, Zhao, T., Pan, X., Zhai, X., Shao, Q., 2018. Simulation and assessment of urbanization impacts on runoff metrics: insights from landuse changes. *Journal of Hydrology* 560, 247–258. <https://doi.org/10.1016/j.jhydrol.2018.03.031>
- Zuo, D., Xu, Z., Peng, D., Song, J., Cheng, L., Wei, S., Abbaspour, K.C., Yang, H., 2015. Simulating spatiotemporal variability of blue and green water resources availability with uncertainty analysis. *Hydrological Processes* 29, 1942–1955.